

Demonstrating flexible operation of the Technology Centre Mongstad (TCM) CO₂ capture plant

Mai Bui^{a,b}, Nina E. Flø^c, Thomas de Cazenove^c, Niall Mac Dowell^{a,b,*}

^a Centre for Process Systems Engineering, Imperial College London, South Kensington, London SW7 2AZ UK

^b Centre for Environmental Policy, Imperial College London, South Kensington, London SW7 1NA UK

^c Technology Centre Mongstad (TCM), 5954 Mongstad Norway

ARTICLE INFO

Keywords:

CO₂ capture
Dynamic modelling
Flexible operation
Transient operation
Post-combustion capture
Pilot plant
CCGT

ABSTRACT

This study demonstrates the feasibility of flexible operation of CO₂ capture plants with dynamic modelling and experimental testing at the Technology Centre Mongstad (TCM) CO₂ capture facility in Norway. This paper presents three flexible operation scenarios: (i) effect of steam flow rate, (ii) time-varying solvent regeneration, and (iii) variable ramp rate. The dynamic model of the TCM CO₂ capture plant developed in gCCS provides further insights into the process dynamics. As the steam flow rate decreases, lean CO₂ loading increases, thereby reducing CO₂ capture rate and decreasing absorber temperature. The time-varying solvent regeneration scenario is demonstrated successfully. During “off-peak” mode (periods of low electricity price), solvent is regenerated, reducing lean CO₂ loading to 0.16 mol_{CO₂}/mol_{MEA} and increasing CO₂ capture rate to 89–97%. The “peak” mode (period of high electricity price) stores CO₂ within the solvent by reducing the reboiler heat supply and increasing solvent flow rate. During peak mode, lean CO₂ loading increases to 0.48 mol_{CO₂}/mol_{MEA}, reducing CO₂ capture rate to 14.5%, which in turn decreases the absorber temperature profile. The variable ramp rate scenario demonstrates that different ramp rates can be applied successively to a CO₂ capture plant. By maintaining constant liquid-to-gas (L/G) ratio during the changes, the CO₂ capture performance will remain the same, i.e., constant lean CO₂ loading (0.14–0.16 mol_{CO₂}/mol_{MEA}) and CO₂ capture rate (87–89%). We show that flexible operation in a demonstration scale absorption CO₂ capture process is technically feasible. The deviation between the gCCS model and dynamic experimental data demonstrates further research is needed to improve existing dynamic modelling software. Continual development in our understanding of process dynamics during flexible operation of CO₂ capture plants will be essential. This paper provides additional value by presenting a comprehensive dynamic experimental dataset, which will enable others to build upon this work.

1. Energy systems of the future – the role of flexible CO₂ capture

Climate change is one of the greatest challenges of the 21st century. A recent IPCC report (IPCC, 2018) indicates that immediate and rapid reductions of greenhouse gas (GHG) emissions is needed in order to limit global warming to 1.5 °C. Carbon capture and storage (CCS) will have an essential role in the deep mitigation of fossil fuel emissions and in CO₂ removal from the atmosphere (IPCC, 2018). The transition to a low carbon energy system requires a large share of intermittent renewable energy (e.g., wind, solar), which presents major operational challenges (Ludig et al., 2010; Heuberger and Mac Dowell, 2018). Thermal power plants with CCS can take on the essential role of providing dispatchable low carbon capacity, crucial in balancing an energy system with high penetration of intermittent renewables (van der Wijk et al., 2014; Boston and Thomas, 2015; Heuberger et al., 2016,

2017a,b,c; Heuberger and Mac Dowell, 2018; Bui et al., 2018a). Thus, flexible operation of both thermal power plants and CO₂ capture plants will be necessary to coordinate the balance between electricity demand and CO₂ emissions reduction targets (Bui et al., 2014a,b, 2016b; Mac Dowell and Shah, 2015; Mac Dowell and Staffell, 2016; Bandyopadhyay and Patiño-Echeverri, 2016; Mechleri et al., 2017).

As the pressure to improve the economic and technical performance of CO₂ capture plants continues to grow, attention is being directed to the development of flexible operation strategies (Gardarsdóttir et al., 2015; Bui et al., 2016b). Flexible operation can maximise profitability by ramping up, ramping down or turning off CO₂ capture in accordance with electricity prices (Cohen et al., 2012). Some proposed flexible operation strategies include variable CO₂ capture rates, bypass or venting systems, solvent storage (Chalmers and Gibbins, 2007; Cohen et al., 2012; Bui et al., 2014a,b), and time-varying solvent regeneration

* Corresponding author.

E-mail address: niall@imperial.ac.uk (N. Mac Dowell).

<https://doi.org/10.1016/j.ijggc.2019.102879>

Received 20 May 2019; Received in revised form 14 October 2019; Accepted 21 October 2019

1750-5836/ © 2019 Elsevier Ltd. All rights reserved.

(Mac Dowell and Shah, 2015). Although studies show that such flexible operation strategies improve the economic viability of CO₂ capture (Zaman and Lee, 2015; Mac Dowell and Shah, 2015; Zaman et al., 2016; Mechleri et al., 2017), there is still a lack of research into the technical effects of process disturbances during flexible operation. Thus, there is a justified need to develop practical experience in dynamic operation of CO₂ capture pilot plants, which can help improve the robustness of flexible operation strategies (Bui et al., 2018b).

Whilst there are ample modelling studies confirming the value of flexible operation, presenting theoretical ideas, and economic analyses, there is a marked absence of pilot plant campaigns which evaluate the feasibility of flexible operation under realistic operating conditions. Furthermore, the development of flexible operation strategies tends to be model-based design and many of these strategies have yet to be demonstrated in CO₂ capture pilot plants (Bui et al., 2014a,b, 2018b). Experimental testing in pilot plants will be vital in demonstrating the feasibility of proposed flexible operation strategies. Additionally, experimental pilot plant data have an important role in the development of robust and accurate dynamic models (Bui et al., 2014a, b). However, acquiring reliable dynamic pilot plant data for model validation is a challenge owing to scarcity. Studies that investigate dynamic or flexible operation in pilot plants will be essential. There are a growing number of publications that report findings from dynamic/flexible operation testing at various pilot plants: (i) CSIRO's CO₂ capture pilot plant at Loy Yang power station (Australia) (Bui et al., 2014a,b, 2016a), (ii) pilot-scale facilities of Sulzer Chemtech (Switzerland) (Tait et al., 2016), (iii) Brindisi capture pilot plant (Italy) (Mangiaracina et al., 2014; Enaasen et al., 2014; Flø et al., 2016), (iv) UKCCSRC PACT pilot plant (United Kingdom) (Tait et al., 2017, 2018), (v) TCM CO₂ capture plant (Norway) (de Koeijer et al., 2014; Montañés et al., 2017; Montañés et al., 2018). Some of these provide useful experimental pilot plant datasets that can be used for dynamic model validation (Mangiaracina et al., 2014; Enaasen et al., 2014; Bui et al., 2016a, 2018b). The development of dynamic CO₂ capture models and dynamic pilot plant experiments has been extensively reviewed in previous contributions (Bui et al., 2014a,b, 2018b), and is therefore not extensively discussed again here.

2. Study objectives: demonstrating the feasibility of flexible operation

Many flexible operation strategies developed in literature have only been evaluated using modelling techniques. Pilot-scale or large-scale plant demonstration of novel operation strategies is an important and essential step in testing the technical feasibility of such strategies. In this work, we developed flexible operation procedures based on concepts designed from modelling work in earlier contributions (Mac Dowell and Shah, 2015; Mechleri et al., 2017). The testing at TCM has provided invaluable operating experience in designing and implementing novel flexible approaches at a CO₂ capture plant. Furthermore, it demonstrates that flexible operation approaches can successfully work in practice, providing certainty around feasible dynamic operating limits for a capture plant. As the availability of dynamic pilot plant data is an area of priority for the development of robust dynamic process models (Bui et al., 2014a,b, 2018b), the detailed dynamic experimental datasets from this work are presented in Appendix and Supplementary Material.

The objective of this work is to demonstrate the feasibility of flexible operation in a large post-combustion CO₂ capture plant. Three flexible operation strategies are investigated: (i) effect of steam flow rate, (ii) time-varying solvent regeneration, and (iii) variable ramp rate. The time-varying solvent regeneration scenario is a unique flexible operation strategy that demonstrates the ability to store CO₂ within the working solvent (Mac Dowell and Shah, 2015; Mechleri et al., 2017), which avoids significant capital investment for additional equipment (e.g., solvent storage tanks) (Van Peteghem and Delarue, 2014; Oates

et al., 2014; Abdilahi et al., 2018). The variable ramp rate scenario investigates the ability to ramp process parameters at different rates, whilst maintaining a constant CO₂ capture performance (i.e., same CO₂ capture rate). Modelling studies demonstrate that these approaches are profitable, with improved techno-economic performance compared to other flexible operating strategies (Mac Dowell and Shah, 2015).

A dynamic process model of the TCM pilot plant is developed using gCCS, and is validated against the TCM plant data. As demonstrated in a previous contribution (Bui et al., 2018b), gCCS models demonstrate good agreement with experimental data from pilot plants.¹ This paper examines the dynamics of a demonstration-scale CO₂ capture plant which captures 80–200 tonnes CO₂/day (Morken et al., 2019). We demonstrate, for the first time, the integration of model-designed process strategies into practical experimental tests at a demonstration-scale capture plant.² By combining both experimental testing with dynamic modelling simulations, this work aims to provide invaluable insight into the detailed process dynamics during flexible operation of a CO₂ capture process.

3. Flexible operation test campaign at Technology Centre Mongstad (TCM)

3.1. Plant description

The Technology Centre Mongstad (TCM) test facility is located next to the Equinor oil refinery in Mongstad, Norway. The TCM amine absorption plant is designed to be flexible with two possible configurations that typically captures 85% of the CO₂ from different flue gas slipstreams (Andersson et al., 2013; Hamborg et al., 2014). At a flue gas volumetric capacity of 60,000 Sm³/h,³ the plant captures about 80 tonnes CO₂/day from the exhaust gas of the natural gas-fired combined heat and power (CHP) plant, which has 3.5–4.1 mol% CO₂ composition (Hamborg et al., 2014). This CHP plant uses a combined cycle gas turbine (CCGT). The configuration that processes flue gas from the refinery residual fluid catalytic cracker (RFCC) of 13 mol% CO₂ composition has the capacity to capture 200 tonnes CO₂/day (Hamborg et al., 2014; Morken et al., 2019). The feed flue gas CO₂ concentration can be varied between 2.5% and 15% by recirculating the dry CO₂ product upstream of the direct contact cooler (i.e., exhaust gas recirculation) (Hamborg et al., 2014; Montañés et al., 2017) or by air dilution of the RFCC gas (Morken et al., 2019). The TCM plant has two direct contact coolers (DCC) and two stripper column units to cater for the two different flue gas streams. The RFCC configuration treats flue gas streams of greater CO₂ composition, thus the dimensions of the RFCC DCC and stripper are larger compared to the CHP configuration (Hamborg et al., 2014). The two stripper units operate independently of each other. The process configuration of the CHP system is shown in Fig. 1.

An induced draft (ID) blower used to blow the flue gas through the plant has a blower output capacity of up to 70,000 Sm³/h. The flue gas is initially quenched, cooled and pre-scrubbed in a direct contact cooler by counter-currently contacting flue gas with water. In the absorber, the flue gas enters from the base of the column and lean solvent flowing counter-currently from the top absorbs CO₂ from the flue gas. The rectangular absorber column is constructed from polypropylene-lined concrete with a cross-section measured at 3.55 m × 2 m and total height of 62 m. Along the lower absorption sections of the column,

¹ The study investigated flexible operation of the UKCCSRC PACT CO₂ capture pilot plant, which has a capture capacity of 1 tonne CO₂/day.

² To the best of our knowledge. For an extensive overview of dynamic/flexible operation test campaigns at CO₂ capture pilot plants, including the dynamic operation scenarios tested experimentally, please refer to Bui et al. (2018b).

³ S denotes standard conditions of 1 atm and 15 °C.

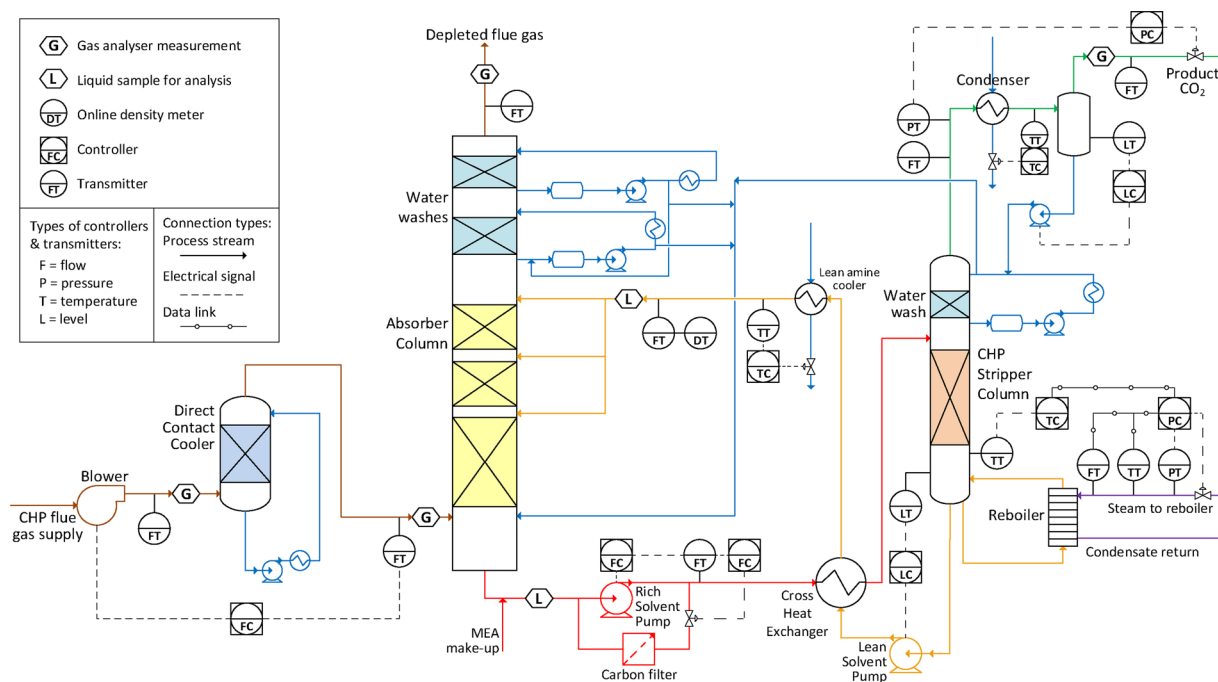


Fig. 1. Process flow diagram of the amine-based CO₂ capture process at TCM when configured to treat flue gas from the combined heat and power (CHP) plant. Some key process control loops are shown, however, much of the detail in the P&ID is omitted, also units upstream and downstream of the capture plant are not shown.

there are three beds of packing with three possible solvent inlet points along the height of the absorber, providing three absorber packing heights: 12 m, 18 m or 24 m (12 m + 6 m + 6 m). As the processed flue gas moves upwards, it passes through the water washes at the top section of the absorber, scrubbing the flue gas and reducing solvent entrainment (minimises solvent loss). The cold water wash has two key purposes: (i) maintain a closed water balance in the solvent system by condensing water vapour in the exit flue gas, and (ii) reduce the concentration of volatile organic compounds, e.g., MEA, or amine degradation products (formaldehyde, acetone, acetaldehyde) (Knudsen et al., 2009), in the depleted flue gas.⁴ The CO₂-depleted flue gas exits the top of the absorber column. Rich solvent exits the bottom of the absorber column and is heated in the cross heat exchanger by a counter-current stream of hot lean solvent.

The rich solvent is directed to one of the two stripper columns – both have a height of 30 m, operating independently with its respective thermosiphon reboiler. Stripper selection is based on CO₂ content and fluid hydraulic effects. The stripper with the smaller diameter of 1.3 m is designed for flue gas with CO₂ content < 6 vol% (e.g., CHP flue gas). The larger stripper of 2.2 m diameter is suitable for feed flue gas with CO₂ content > 4 mol%. The reboiler temperature varies between 110 and 125 °C, where heat is supplied by steam at 140–160 °C. As rich solvent flows down the stripper column, the desorption of CO₂ from the solvent generates a lean solvent stream (exits the bottom) and CO₂ product (exits top of the column). The lean solvent is cooled in the cross heat exchanger (by low temperature rich amine), and further cooled by the lean amine cooler at the absorber inlet. The CO₂ product exiting the top passes through the condenser and reflux drum (removes entrained droplets) before being sent to the CO₂ stack (Hamborg et al., 2014; Thimsen et al., 2014; Montañés et al., 2018).

3.2. Description of the flexible operation strategies

The flexible operation test campaign was conducted in July 2017,

⁴ The loss of MEA via emissions to air is typically insignificant compared to loss due to amine degradation.

using the combined heat and power (CHP) plant configuration (flue gas CO₂ content of 3.5–4.1 mol%) with 30 wt% monoethanolamine (MEA) aqueous solution and a packing height of 24 m in the absorber column. The column specifications of the absorber and CHP stripper configuration used for this test campaign are provided in Table A.2 (Appendix A). The operating window of key process parameters during the flexible operation test campaign is summarised in Table 1. As part of this campaign, three flexible operating scenarios were tested on behalf of Imperial College London (ICL). Fig. 2 illustrates the change in process parameters as the flexible operation scenarios were implemented at the TCM CO₂ capture plant. At each time period (e.g., ICL₁, ICL₂), process parameters are adjusted to new process conditions, the TCM plant subsequently runs for 3–5 h in order to stabilise the process and reach a new steady state.⁵ The actual times at which process parameter changes were implemented are given in Appendix C, Table C.5, and are shown in Fig. 2 as vertical grey lines labelled ICL₁ to ICL₁₃.

3.2.1. Effect of steam flow rate (ICL₁ to ICL₆)

The first phase will provide results to understand the process dynamics of changes to steam flow rate alone. As shown in Fig. 1, the positioning of the steam pressure valve is adjusted to achieve the desired steam flow rate, i.e., steam flow rate is not being directly controlled. Steam flow rate is important for the entire CO₂ capture process as it dictates the overall temperature of the system, and importantly, the reboiler and stripper temperature (controlling the degree of solvent regeneration). The impact of steam flow rate on the reboiler temperature is shown for the entire test campaign in Appendix C.4. If the stripper section cools down, this would result in an overall cooling of the absorption section, which potentially influences the kinetics of CO₂ absorption. It is unlikely that the effect on kinetics will be observable in the plant data but it is important to establish this relationship between steam flow rate and degree of capture (DoC).

The steam flow rate range for stable operation of the CHP stripper

⁵ The TCM plant is able to stabilise within one hour for 20% step changes in process inputs (Montañés et al., 2018). However, a minimum of three hours was provided to ensure homogeneous composition in the solvent samples.

Table 1

The operating ranges for key process parameters during the test campaign at the TCM CO₂ capture plant. Flue gas blower can reach a maximum output capacity of up to 70,000 Sm³/h. DCC = direct contact cooler, L/G = liquid-to-gas.

Parameter	Unit	Range
Flue gas flow rate	Sm ³ /h	30,000–60,600
Flue gas temperature (after DCC)	°C	30
Flue gas CO ₂ concentration	vol%	3.6–4.1
Lean solvent flow rate	kg/h	28,200–60,100
Lean solvent temperature	°C	37.0
L/G ratio	kg liquid/Sm ³ gas	0.71–1.27
CO ₂ capture rate ^a	%	14–97
MEA concentration	wt%	26–28
Absorber packing height	m	24
Stripper bottom pressure	Bar _a	1.9–2.0
Steam temperature	°C	140.6–158.5
Reboiler temperature	°C	109.5–124.2
Reboiler heating rate	MJ/h	2260–11,890
Steam flow rate for stable operation of CHP stripper reboiler	kg/h	1000–5000

^a CO₂ capture rate average from the four calculation methods.

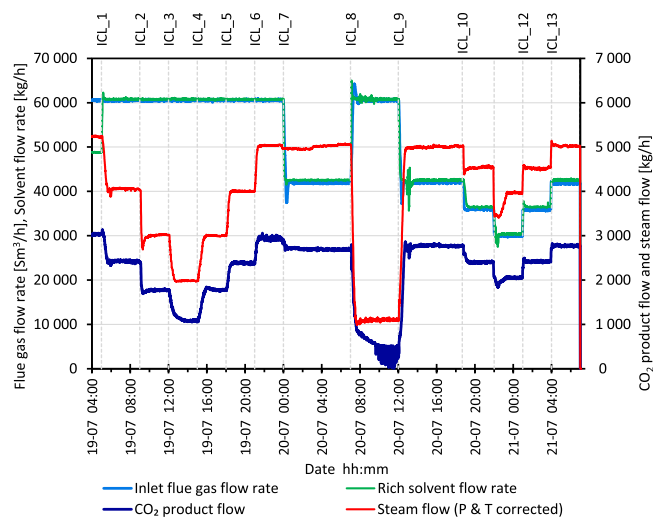


Fig. 2. Process parameter changes during the flexible operation campaign in July 2017 at the TCM CO₂ capture plant. The three flexible operation scenarios tested (i) effect of steam flow rate (ICL₁ to ICL₆), (ii) time-varying solvent regeneration (ICL₇ to ICL₉), and (iii) variable ramp rate (ICL₁₀ to ICL₁₃).

was between 1000 and 5000 kg/h. A series of step changes⁶ to the steam flow rate was conducted (4000, 3000, 2000, 3000, 4000 and 5000 kg/h) and the resulting lean CO₂ loading measured. As the subsequent time-varying solvent regeneration scenario involved simultaneous changes to multiple plant parameters, this data was useful in determining the degree of change in lean CO₂ loading that arose from changing only the steam flow rate. Understanding and quantifying the impact of steam flow rate on plant performance was necessary to adequately evaluate performance of the time-varying solvent regeneration scenario.

3.2.2. Time-varying solvent regeneration (ICL₇ to ICL₉)

Although solvent storage is shown to be a promising approach, it involves high capital cost due to the use of large storage tanks (Van Peteghem and Delarue, 2014; Oates et al., 2014; Abdilahi et al., 2018; Husebye et al., 2011). A potentially more cost effective approach is using the time-varying solvent regeneration approach, first proposed by Mac Dowell and Shah (2015). During the periods of high electricity

price, less steam is directed to solvent regeneration (from the steam cycle), enabling the power plant to increase electricity output. The CO₂ is stored to accumulate in the amine absorbent, which enables the “storage” of CO₂ within the solvent. As shown by previous modelling work, lean loading subsequently increases, whilst the degree of capture (DoC) simultaneously decreases. Conversely, the solvent is regenerated during off-peak electricity prices (i.e., steam flow is restored to the reboiler), increasing the degree of capture and reducing the lean CO₂ loading (Mac Dowell and Shah, 2015; Mechleri et al., 2017).

A novel experimental test procedure for the TCM plant was designed to demonstrate this time-varying solvent regeneration approach as: (i) a “peak” mode, and (ii) an “off-peak” mode. In the “peak” mode of operation, steam flow to the reboiler was reduced. It is expected that during peak electricity prices, the higher electricity output would result in an increase flue gas flow rate (due to higher rates of fuel firing). For “off-peak” operation, steam flow rate was increased and flue gas flow rate reduced. During testing, the changes to process parameters (flue gas flow rate, solvent flow rate and steam flow rate) were implemented as step changes.

3.2.3. Variable ramp rate (ICL₁₀ to ICL₁₃)

In the development of flexible operation strategies, an important consideration is plant flexibility, which depends on: (i) the achievable minimum load, and (ii) ramp rate capabilities. Conventional combined cycle gas turbine (CCGT) power plants have ramp rates that range between 2–8%P_n/min (percentage of the nominal load per minute), whereas the ramp rate of gas turbines is between 8 and 15%P_n/min (Hentschel et al., 2016). Although the power plant ramp rate limits are relatively well understood, there is a lack of reliable data on ramp rate limits for CO₂ capture processes. The ramp rate is a key process parameter that can limit the flexibility of a CO₂ capture plant. Thus, evaluation of the ramp rate limits of a capture plant in comparison to those of a power plant was necessary in designing realistic flexible operation strategies.

The objective of this scenario was to demonstrate and test achievable ramp rates (i.e., an indicator of plant flexibility) in the TCM CO₂ capture plant. Due to limitations in the operating window of key process parameters (flue gas flow rate and steam flow rate), the ramp rates tested were conservative compared to typical CCGT ramp rates. As the inlet flue gas flow rate was ramped up/down, liquid flow rate was adjusted simultaneously at the same ramp rate to maintain a constant degree of capture (maintain constant L/G ratio).

3.3. Experimental measurements and data processing

A detailed description of the measurement instruments used to monitor stream conditions and composition is available in previous contributions (Andersson et al., 2013; Brigman et al., 2014; Hamborg et al., 2014; Thimsen et al., 2014; Faramarzi et al., 2017), which also include a detailed analysis of measurement accuracy, bias and precision (i.e., quantification of uncertainty and error). Temperature, pressure and flow rate are measured throughout the pilot plant and logged every 30 s. Measurement precision and uncertainty of gas composition at TCM has been recently quantified and reported in Faramarzi et al. (2017). Gas phase composition is monitored with the use of multiple gas measurement systems, combined, these ensure continuity of data and provide a means to assess measurement uncertainty. Two Gasmet Fourier transform infrared (FTIR) and one AIT⁷ FTIR gas analysers supply continuous measurements of CO₂, H₂O, NH₃, NO, NO₂, SO₂, CH₂O, C₂H₄O, MEA. The gas chromatograph (GC) measures composition of CO₂, O₂, N₂, H₂O.⁸ Additionally, five non-dispersive infrared

⁷ Applied Instrument Technologies.

⁸ Gasmet FTIR analysers are located at the flue gas absorber outlet and CO₂ product stream, whereas the AIT FTIR is located at the flue gas absorber inlet. These three gas streams are also analysed by the GC.

⁶ Steam flow was immediately changed to the set-point setting in one step.

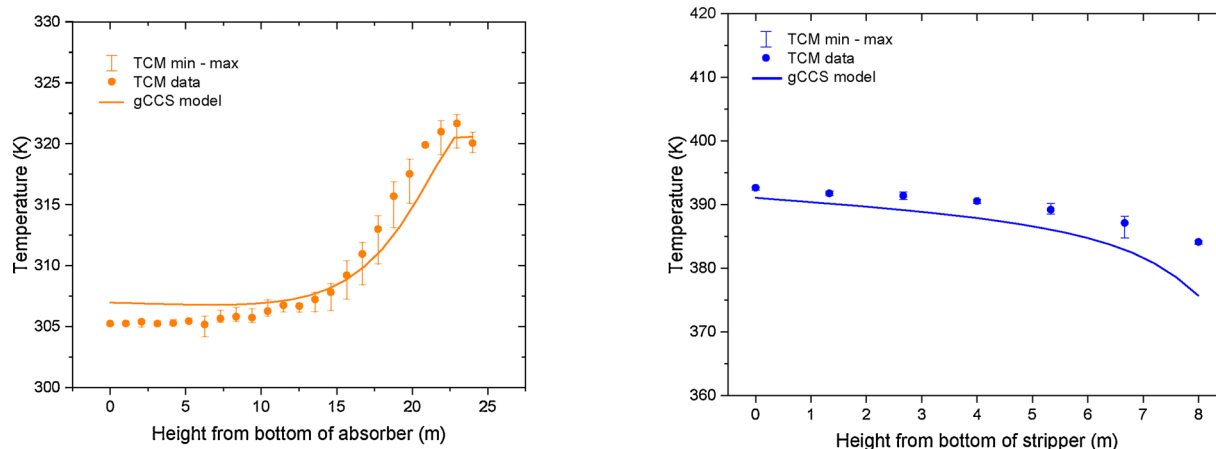


Fig. 3. The temperature profiles for the absorber column (left) and the stripper column (right) at “initial” conditions 18/07/2017 22:00, before the campaign commences. One point on the profile represents the mean temperature from the 4 sensors at a given height of packing (distributed radially) and whiskers show the minimum and maximum.

(NDIR) are used for CO₂ content: two at the absorber inlet (low and high gas CO₂ concentration), two at the absorber outlet and one analysing the CO₂ product. A trace O₂ analyser is used to measure O₂ levels in the CO₂ product (Faramarzi et al., 2017). Combining this data together provides detailed gas phase composition at three locations – absorber gas inlet (base), absorber gas outlet (top), and the product CO₂ (top of stripper), shown in Fig. 1.

For this dynamic test campaign, monitoring the transient behaviour of the liquid phase CO₂ composition is essential. The lean and rich CO₂ loading of the solvent was measured using two approaches: (i) manual off-line titration of solvent samples collected periodically, and (ii) continuous online method using the density meters and a correlation. For the off-line method, manual samples of the solvent were collected at the inlet and outlet liquid streams of the absorber. Chemical liquid analysis of these samples provide solvent composition, including CO₂ loading and MEA concentration. The laboratory could only accommodate a limited number of chemical samples for analysis per day. Thus, specific solvent sample locations (e.g., lean or rich) and time periods (e.g., ICL7) essential for model validation were prioritised for chemical analysis, hence, some manual lean/rich loading measurements are absent (Fig. 5 and Table C.9). Additionally, online density meter measurements are available for the inlet solvent stream of the absorber. By using a correlation derived from a previous MEA test campaign, the instantaneous CO₂ loading is calculated based on the density meter measurements, providing the dynamic trends of CO₂ loading. Fig. 5 shows the change in CO₂ loading over the course of the test campaign, where circular points correspond to chemical analysis measurements at the specific times of solvent sampling, and the blue line represents calculated online lean loading.

The temperature profiles in the absorber and stripper columns are particularly important indicators of plant performance. Thus, these measurements will be essential for dynamic model validation. Pilot plants typically have a single temperature transmitter at a given column height. The TCM CO₂ capture plant has four temperature transmitters distributed radially at each metre along the height of the absorber column, resulting in a total of 96 temperature sensors, providing more detail for temperature profiles. Along the 8 m height of the stripper column, there are 28 temperature sensors in total, four for every 1.14 m of packing. The temperature at a given height of the profile is shown as a mean of the 4 sensors with whiskers to indicate the minimum and maximum (Fig. 3). This approach is distinct to previous studies of the TCM plant, which typically only show the mean temperature of the 4 sensors. Uncertainty in the experimental data and model will influence the model validation results (Bui et al., 2018b). Temperature representation in this format (i.e., min–mean–max) quantitatively

illustrates variation/uncertainty in the experimental data, which is a better indication of model validation. The uncertainty in the TCM CO₂ capture rate based on the four different calculation methods (Appendix B.2) can also be shown. In this study, a solid orange line represents the average TCM CO₂ capture rate and the orange shaded region surrounding this line illustrates the variance between the minimum and maximum values (e.g., Fig. 10).

Temperature transmitter and flow rate measurements are particularly prone to noise or instability under certain operating conditions at specific locations. The presence of two phases (i.e., liquid, gas) could contribute to noise; there are many instances when this can occur. Within the absorber column, liquid amine and flue gas (two phases) are present, with the liquid gathering at the liquid redistribution plates to be redistributed evenly over packing (Bui et al., 2016a). In the stripping section, “degassing” of CO₂ gas bubbles out of the liquid may occur under certain operating conditions. Two-phase flow patterns (e.g., bubble, slug, plug, annular) may occur within piping at certain liquid flow rates. In these instances, as the volume surrounding the probe shifts from measuring the gas phase to the liquid phase, there will be observable fluctuations in the measurement data, e.g., flow rate, temperature, pressure or density. Positioning of probes specifically designed for single phase applications (i.e., liquid only) is particularly important in preventing noise. Other possible sources of noise include electrical, mechanical vibration or process noise. There tends to be more noise during flexible operation as the plant deviates from the design conditions and specifications.

Noisy data needs to be processed before they can be used to calculate other process parameters (e.g., CO₂ capture rate) and for model validation. Approaches include: (i) use another similar measurement as an analogue (e.g., an adjacent temperature transmitter), or (ii) apply noise reduction techniques directly to the dataset (i.e., smoothing filter). Unless there is evidence that the integrity of measurements has been compromised, omitting noisy measurement data from the final results/dataset is not recommended. The following section describes the approach for noise reduction of data used to calculate lean CO₂ loading.

3.4. Online CO₂ loading correlation

The ability to monitor transient behaviour in the liquid phase is essential for dynamic pilot plant testing (Bui et al., 2016a,b; Tait et al., 2016). The following correlation is used to calculate online CO₂ loading from measurements of lean amine density and temperature at the absorber inlet (Fig. 4). This correlation was developed during a previous TCM test campaign that used MEA solvent without an oxygen

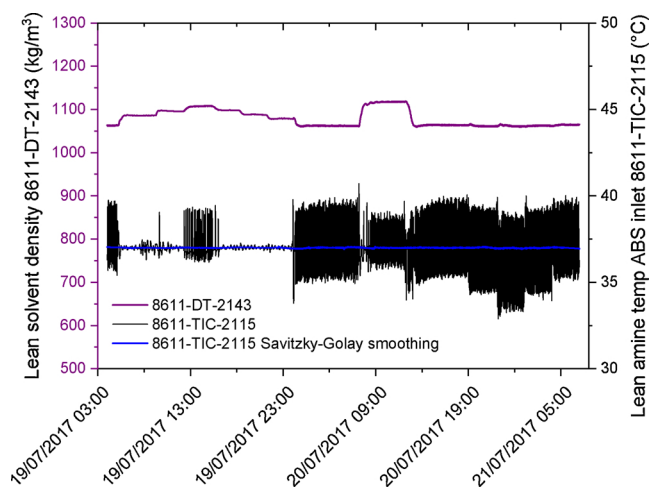


Fig. 4. Lean solvent density DT-2143 measurements (purple line) and lean absorber inlet temperature [TIC-2115] are used to calculate the lean CO₂ loading. Due to the noise in measurements from TIC-2115 (black line), the Savitzky-Golay method is used to smooth the data (blue line). (For interpretation of the references to colour in this figure legend, the reader is referred to the web version of this article.)

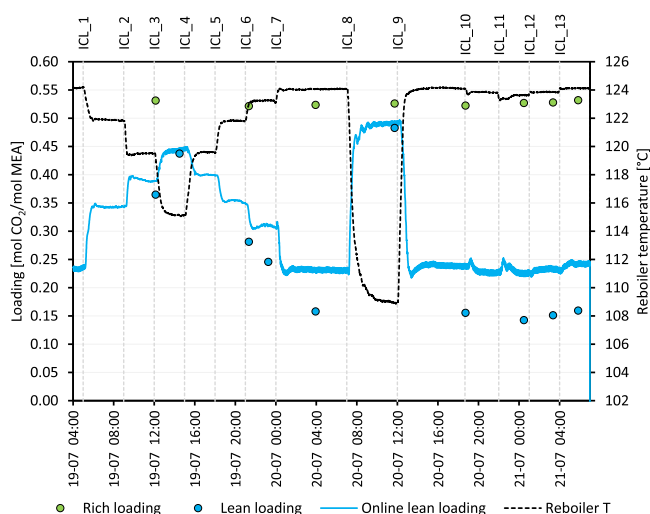


Fig. 5. CO₂ loading as a function of reboiler temperature (black line). The blue and green points are chemical analysis measurements of rich/lean CO₂ loading (manually sampled). The blue line is the calculated online lean loading based on density meter measurements. (For interpretation of the references to colour in this figure legend, the reader is referred to the web version of this article.)

scavenger. This test campaign used MEA solvent with an oxygen scavenger (details published (Morken et al., 2019; Flø et al., 2019)). Consequently, the online density correlation method tends to overestimate lean loading compared to the off-line titration measurement (Fig. 5). The deviation reduces for higher lean loading, e.g., ICL₃ and ICL₈, where the off-line and calculated online method are in close agreement. In this study, the manual off-line titration measurements were used for model validation, whereas calculated online lean loading provided an indication of the transient trends:

$$[DT-2143] = 214.0181 \times \text{Lean CO}_2 \text{ loading} - 0.985671951 \times [TIC-2115] + 1049.033 \quad (1)$$

$[DT-2143]$ = lean solvent density (kg/m³) measurement from density meter 8611-DT-2143; $[TIC-2115]$ = temperature of cooled lean amine at absorber inlet (°C), measured by 8611-TIC-2115.

Across the different operating conditions during this test campaign, measurements from the temperature transmitter 8611-TIC-2115

exhibits noise, fluctuating significantly between 33 and 41 °C, as shown by the black line in Fig. 4. Thus, data smoothing needs to be applied to the raw data from 8611-TIC-2115 before it is used to calculate the online lean CO₂ loading (using Eq. (1)). The graphing and data analysis software Origin provides multiple smoothing methods/tools, including Adjacent Averaging, Savitzky-Golay, Percentile Filter, FFT Filter, Lowess and Loess. Each of these smoothing methods perform differently depending on the nature of the noise.

As the Savitzky-Golay (SG) filter preserves the features of the data (e.g., peak height and width) and overall profile, SG was used to smooth the data from temperature transmitter 8611-TIC-2115. Appendix D provides further information about each smoothing method, also Figs. D.21 and D.22 illustrate the effect of data smoothing. Although the raw data for lean amine temperature [8611-TIC-2115] fluctuates significantly, the smoothed dataset remains constant at 37 °C, with the exception being the Percentile Filtering method which exhibits perturbations. In contrast, the dataset for the density meter 8611-DT-2143 did not require any smoothing. The smoothed data for temperature transmitter 8611-TIC-2115 shown in Fig. 4 are used to calculate the online lean CO₂ loading in this study (shown in Fig. 5).

3.5. Model validation against TCM results

For model validation, predictions from the dynamic model will be compared against TCM pilot plant results from the flexible operation campaign. The performance of the dynamic operation scenarios will be evaluated in terms of:

- Absorber and stripper column temperature profiles.
- Lean and rich CO₂ loading: ratio of the moles of CO₂ to moles of amine (Fig. 5); used to monitor the amount of CO₂ absorbed in the solvent (the amount on a mass basis of CO₂ “stored” in the solvent was also determined, refer to Table C.15).
- CO₂ capture rate %: quantifies the performance in terms of the proportion of CO₂ that is captured from the feed flue gas.
- Reboiler duty (specific thermal duty): provides information on the thermal energy requirements on a MJ per kg CO₂ basis (Fig. 6).

For some performance indicators, there are multiple calculation methods. This work considers two types of CO₂ capture rate: (i) instantaneous CO₂ capture rate (Fig. 6) calculated continuously with online measurements (simply referred to as the CO₂ capture rate), and

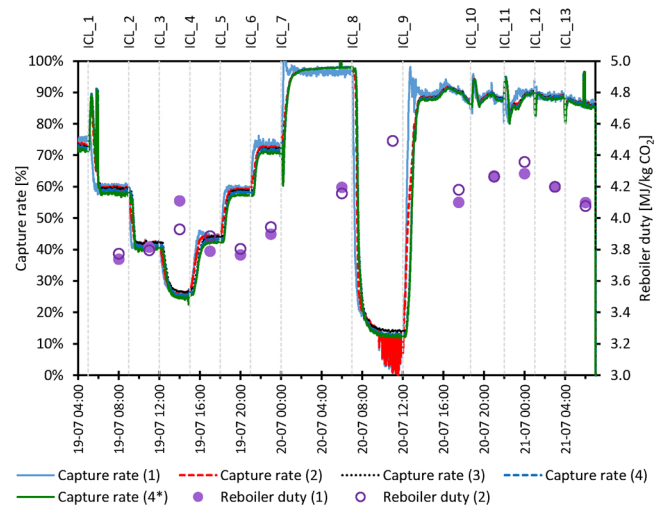


Fig. 6. CO₂ capture rate and the average reboiler duty during the TCM test campaign (calculation methods in Appendix B). The result values are presented in Table C.9. Reboiler duty method 1 for ICL₈ is an outlier, thus it has been excluded.

(ii) cumulative CO₂ capture rate (data available in Appendix C.5), which is calculated from the cumulative amount of CO₂ over a duration of time (e.g., over an entire scenario or time period such as ICL_2). More details about the calculation methods are provided in Appendix B.⁹ The TCM experimental results are used to validate the model under steady state and dynamic conditions. As discussed in Section 3.3, the format of absorber and stripper temperature measurements is unique. The min–max temperature range also provides insight into the measurement quality, i.e., a large min–max range would indicate high levels of noise or a wide variation between the 4 transmitters at that column height. Fig. 3 shows that this model validation approach provides more insight on the degree of agreement; model predictions may not precisely match the mean value but may be within the min–max range.

4. Developing a dynamic model of the TCM CO₂ capture process

4.1. Dynamic model description

A dynamic flowsheet model of the TCM CO₂ capture plant was developed in the software gCCS (PSE, 2017), designed for whole chain CCS systems modelling (Rodríguez et al., 2014). The model can simulate both steady state and dynamic process condition. The absorber and stripper columns are modelled using the rate-based approach with the Billet correlation (structured or random packing) (Billet and Schultes, 1993) for the mass transfer model. The TCM column specifications, dimensions and packing information are provided in Table A.2. Dynamic process models also require the specification of equipment volumetric capacity (e.g., column sump volume) to accurately describe the process dynamics; detailed in the PSE gCCS model documentation (PSE, 2016). Appendix C presents the TCM steady state and dynamic plant data that was used to specify the equipment and feed stream conditions in the TCM model. Some of the key model input specifications include composition, flow rate and temperature of the feed streams (i.e., supply flue gas and lean solvent entering the absorber).

The gCCS model employs the gSAFT physical properties package to describe the thermophysical properties of the process fluids. This property package implements the statistical associating fluid theory (SAFT) (Chapman et al., 1989, 1990) with two equations of state (EOS) available: (i) SAFT-VR Square Well (SAFT-VR SW) (Gil-Vilegas et al., 1997; Galindo et al., 1998), and (ii) SAFT- γ Mie (Lafitte et al., 2013; Papaioannou et al., 2014). The thermodynamics and fluid-phase equilibria for the chemical absorption of CO₂ by an amine solvent are specifically described with gSAFT, using SAFT for potentials of variable range (SAFT-VR). The validation of this thermodynamic model is presented in previous studies (Mac Dowell et al., 2010, 2011; Rodríguez et al., 2012; Brand et al., 2012; Brand, 2013).

Fig. 7 illustrates the dynamic model flowsheet in gCCS based on the configuration of the TCM CO₂ capture plant. The TCM plant equipment specifications and operating conditions that have been used to configure the gCCS model are available in Appendices A and C.

4.2. Steady state validation of the dynamic model

Two steady state datasets from earlier test campaigns at the TCM CO₂ capture facility were used to validate the dynamic model at steady state conditions: (i) 2014 baseline data (80% operating capacity) (Hamborg et al., 2014), and (ii) 2015 baseline data (100% operating capacity) (Faramarzi et al., 2017). The difference between the two steady state cases in terms of process conditions is shown in Appendix C. The key characteristics that distinguishes the two baseline cases are: (i) the 2014 baseline settings results in higher CO₂ capture rate of 95%,

whereas the 2015 baseline results in 80% capture; (ii) the 2015 baseline plant settings achieves lower reboiler duty of 3.6 MJ/kg CO₂ (compared with 4.1 MJ/kg CO₂ in 2014).

The shape of the absorber temperature profile provides a good indication of the absorption/capture performance of the process. The key process factors that determine the profile shape and location of the temperature bulge are: flue gas CO₂ content, L/G ratio, solvent properties (e.g., heat of absorption) and packing height (Kvamsdal and Rochelle, 2008). The temperature bulge typically shifts closer to the top of the absorber with decreased L/G ratio, increased packing height, or higher flue gas CO₂ concentration (Kvamsdal and Rochelle, 2008). In comparison with the 2014 baseline (Fig. 8), the temperature bulge of the 2015 baseline is closer to the top of the absorber as it operates at a lower L/G ratio (left graph of Fig. 9).

The absolute percentage deviation (APD) is used to indicate the degree of deviation between the pilot plant data and model predictions (defined in Appendix B) (Bui et al., 2018b). Table C.6 shows the APD of predicted process variables compared to TCM data. The gCCS model provides accurate predictions of the 2014 baseline case, within a deviation (APD) of 0.07–3.9%. Fig. 8 shows the gCCS modelled absorber temperature profile is in good agreement with the TCM data, where predictions are within 1% average APD (Table C.7 shows the average absolute deviation to be 3.1 K). In comparison, the deviation of model predictions for the 2015 baseline case were higher (2.8–15.9%). The predicted solvent CO₂ loading had the greatest deviation from TCM data. Consequently, the location of the temperature bulge for the gCCS absorber profile is poorly predicted. However, deviation between the predicted temperature and TCM data is still relatively low (Fig. 9). The average absolute deviation of the modelled absorber profile is 2.9 K, whereas the stripper profile is 2.3 K. Thus, steady state model validation demonstrates that the gCCS model provides a robust description of the underlying physics of this system.

5. Flexible operation of the TCM CO₂ capture plant

This section presents and examines the experimental and modelling results from the three flexible operation scenarios tested at TCM. The plant had been running at steady state conditions for 7 h; “Initial” process conditions are provided in Table C.8. The Imperial College London (ICL) test scenarios start at time period ICL_1, finishing at the end of ICL_13 (times in Table C.5).

To support dynamic modelling analysis by others, this paper presents detailed TCM plant results from the flexible operation test campaign. The online TCM plant data of key process parameters (e.g., flue gas flow rate, solvent flow rates, column temperatures, data uncertainty) are also provided in the Supplementary Material. For each scenario and time period, the steady state plant conditions and capture performance are presented in Appendix C, Tables C.8–C.11. These values represent the average conditions calculated with data from the steady state period. start and end times shown in Table C.5.

The 2015 baseline settings (presented in Table C.6) are considered to be the “optimal” process conditions in terms of having minimal energy consumption (i.e., specific reboiler duty). The following dynamic plant results provide reboiler duty changes across the different dynamic scenarios. Fig. 6 shows that reboiler duty varied between 3.7 and 4.5 MJ/kg CO₂ during the flexible operation test campaign. Reboiler duty is a function of L/G ratio and the stripper conditions. The L/G ratios of the time periods ICL_1, ICL_2, ICL_5 and ICL_6 were similar to the 2015 baseline settings of 0.96–0.97 kg liquid/Sm³ gas, thus, these had the lowest reboiler duty over the test campaign. As the plant settings deviated from the L/G ratio of the 2015 baseline, reboiler duty would increase, e.g., during ICL_3 and ICL_7 to ICL_13. There was some pressure loss over the stripper packing for cases ICL_1 to ICL_6 and ICL_8, which indicates that the stripper could be operating slightly outside optimum conditions, possibly contributing to a slight increase in specific reboiler duty.

⁹ The gCCS model also uses the same calculation methods in Appendix B – method 1 calculation of specific reboiler duty, and method 3 calculation of CO₂ capture rate.

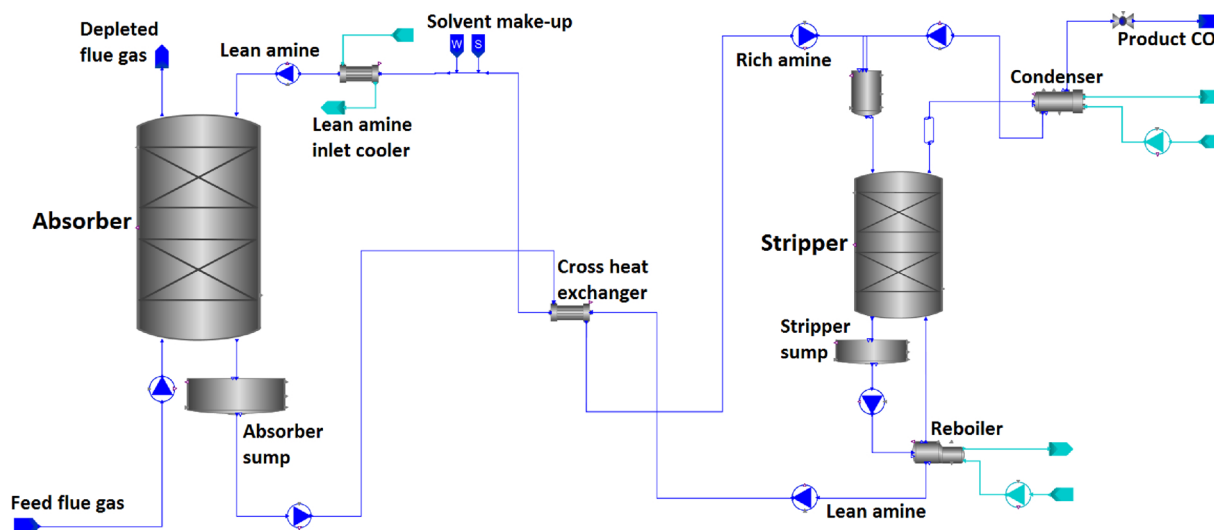


Fig. 7. Dynamic model of the TCM CO₂ capture plant developed in gCCS.

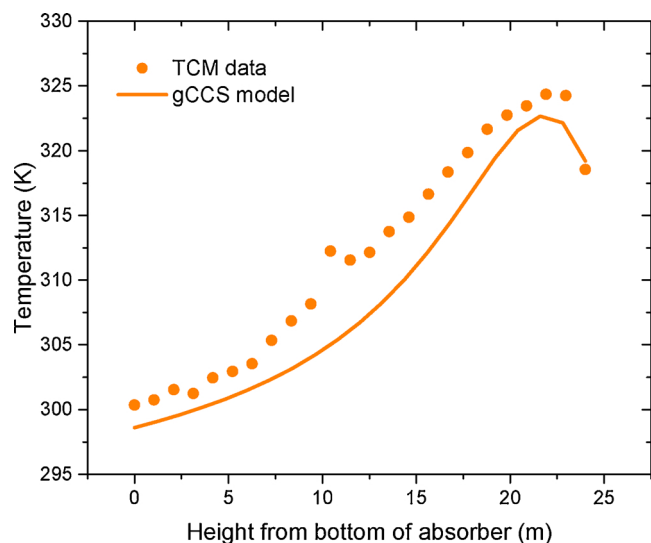
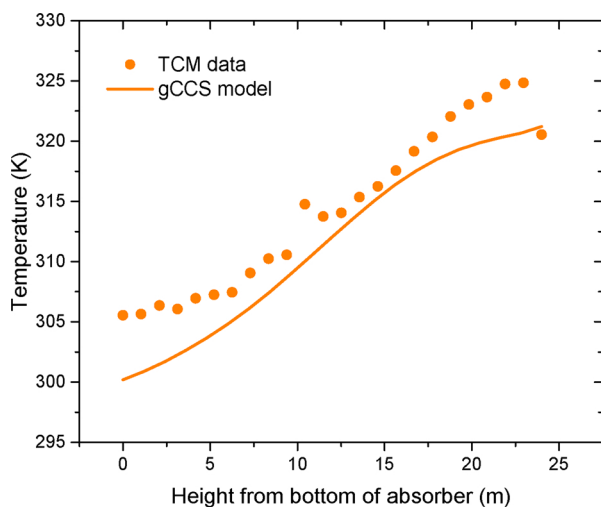


Fig. 8. Steady state TCM absorber temperature validated against gCCS model predictions of the baseline 2014 scenario (Hamborg et al., 2014).



The CO₂ product flow rate decreased continually and fluctuated over the whole time period of ICL₈ (Fig. 2). Consequently, for time period ICL₈, the calculation methods considering CO₂ product flow rate (i.e., specific reboiler duty method 1, and CO₂ capture rate methods 1 and 2) also exhibits similar fluctuations in the trends (Figs. 6 and 13). Other factors that influence comparability of results include the CO₂ concentration of the flue gas and the MEA concentration. As shown in Table C.8, the flue gas CO₂ content at the absorber inlet varies over the course of the test campaign, starting at 3.6 vol% (wet) and increasing to 4.1 vol% (wet). In this study, the MEA concentration of 25.5–28.0 wt% (solvent including CO₂) was slightly lower compared to previous 2014 and 2015 baseline results, which averaged 30 wt% MEA concentration. Any variations in flue gas and MEA solvent concentration would influence CO₂ capture performance, hence, these variations were considered in the dynamic modelling for this paper.

5.1. Effect of steam flow rate

Step changes to the steam flow rate were implemented and the process dynamics of the TCM plant in response to these changes were observed. This scenario studies the effect of changing steam flow rate

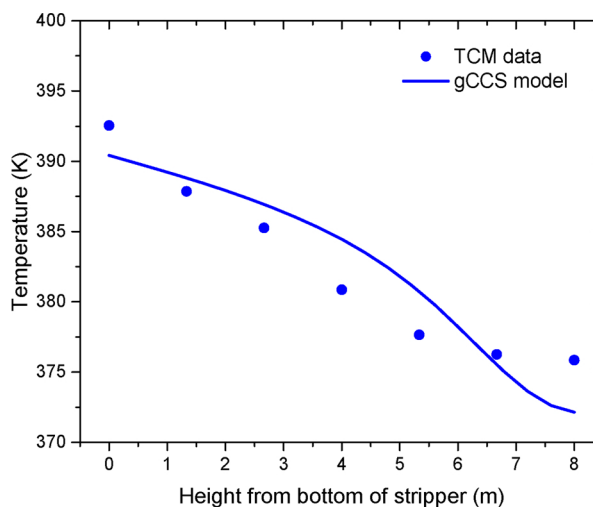


Fig. 9. Steady state TCM absorber (left) and stripper (right) temperature validated against gCCS model predictions of the baseline 2015 results (Faramarzi et al., 2017).

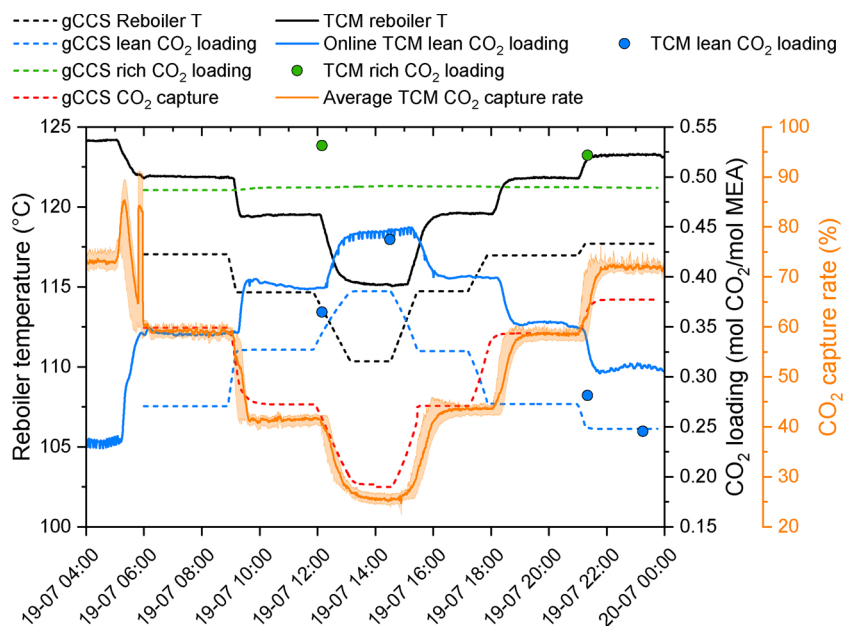


Fig. 10. The effect of steam flow rate scenario – the gCCS model results (dotted lines) in comparison with TCM process measurements (solid lines and points). There are four calculation methods for TCM CO₂ capture rate, the solid orange line shows the average TCM CO₂ capture rate and the shaded orange region illustrates the variance between the minimum and maximum values.

alone, which is an important parameter as it dictates the degree of CO₂ capture. Quantifying the dynamic response to steam flow changes is essential in understanding the dynamic performance of the following flexible operation strategies.

The stripper bottom temperature is a function of the steam flow rate to the reboiler (i.e., increasing steam flow directly increases the stripper bottom temperature), which in turn, affects the lean CO₂ loading and CO₂ capture rate, illustrated in Fig. 10. The steam flow rate was adjusted as step changes as it is controlled by a pressure valve, i.e., one immediate change to the set-point. However, the actual steam flow rate changes were not immediate, occurring as very rapid ramps in Fig. 2. The reboiler required a duration of time to reach the final reboiler temperature (Table C.14), thus, the TCM data shows reboiler temperature changing as ramps. To capture this ramp effect in the dynamic model simulation, reboiler temperature changes were implemented as rapid ramps of similar ramp rate (Fig. 10). The reboiler temperature in the gCCS model was adjusted to be lower than the TCM data. This was necessary in order to compensate for heat loss effects so the gCCS model could achieve a comparative CO₂ capture performance. There is good agreement between the model and experimental TCM data, in particular, the trends of the CO₂ capture rate, manual off-line lean loading, rich loading, reboiler duty and the stripper temperature profiles (APD presented in Tables C.12 and C.13).

As steam flow rate changes in Fig. 11, the absorber temperature profile shape changes and the location of the temperature bulge shifts. The “initial” time period has low L/G ratio of 0.75 kg liquid/Sm³ gas, which resulted in a temperature bulge at the absorber top. As L/G ratio increased for the following time periods (0.95–0.99 kg liquid/Sm³ gas), the absorber temperature bulge shifted slightly down the column. The experimental absorber profiles have the temperature bulge at the top, then the temperature decreased to remain relatively low and constant from the centre to the base of the column. This suggests that most of the CO₂ in the flue gas is absorbed at the top, where the lean MEA solvent enters the absorber column. In contrast, the gCCS model assumed that some CO₂ was absorbed at the top and absorption continued down to the bottom of the absorber. Consequently, some of the temperature profiles have a large absolute error at the middle section of the column (e.g., ICL₁, ICL₂). The average absolute deviation between the TCM data and gCCS predictions is between 1.4 and 4.3 K for the absorber temperature, and 1.7–3.7 K for the stripper temperature (Table C.13).

As the steam flow rate reduces as step changes, the temperature of the reboiler reduced accordingly, hence the reboiler heating rate (MJ/

h) also decreases as step changes, as shown by Fig. C.19. Therefore, the stripper temperature profile shifted downward to lower temperatures – observed in both the TCM plant and dynamic modelling results (left graph of Fig. 12). Consequently, the degree of solvent regeneration in the stripper decreased and lean CO₂ loading increased (Fig. 10). The CO₂ absorption reaction is exothermic. Thus, the increase in lean loading reduced the degree of CO₂ absorption, which decreased the absorber column temperature (left graph, Fig. 11) and CO₂ capture rate. Fig. C.19 shows this corresponds to increased CO₂ flow in the depleted gas stream and decreased CO₂ product flow rate. At the lowest steam flow rate of 2000 kg/h (corresponds to ICL₃), the CO₂ capture rate reduced to 26% and lean loading increased to 0.44 mol_{CO₂}/mol_{MEA}. The CO₂ product flow rate was lower (~1100 kg/h) and reboiler duty was higher at 3.93–4.11 MJ/kg CO₂ (Fig. 6).

Conversely, increasing steam flow rate resulted in higher stripper temperature (right graph, Fig. 12), which reduced lean CO₂ loading and increased CO₂ capture rate. Although reboiler heating rate was greater, the reboiler duty on a MJ/kg CO₂ basis reduced slightly. The lower lean loading led to increased CO₂ absorption, shifting the absorber temperature profile higher (right graph, Fig. 11). The CO₂ product flow rate increased, thereby reducing CO₂ in the depleted flue gas. For example, increasing the steam flow rate to 5000 kg/h (ICL₆), resulted in a CO₂ capture rate of 72% and reduced the lean loading to 0.25 mol_{CO₂}/mol_{MEA}. This led to increased CO₂ flow rate (2900 kg/h) and lower reboiler duty (3.90–3.94 MJ/kg CO₂). Note, despite the changes in steam flow rate, the rich CO₂ loading remained relatively constant (0.52–0.53 mol_{CO₂}/mol_{MEA}) over the duration of this scenario.

5.2. Time-varying solvent regeneration

Fig. 13 illustrates the time-varying solvent regeneration scenario, which began in the “off-peak” mode (ICL₇), before switching to “peak” mode (ICL₈) and back to “off-peak” mode (ICL₉). The time-varying solvent regeneration scenario was particularly challenging to model in gCCS as the “peak” mode experimental conditions were outside the normal window of operation within the gCCS software. Achieving high lean loading close to the rich loading, i.e., 0.48–0.50 mol_{CO₂}/mol_{MEA} (Fig. 13), was not feasibly modelled through steam flow rate or reboiler temperature changes. Alternatively, the process was modelled in a decoupled column configuration (i.e., stand-alone columns) and the measured lean loading was used as a model input for dynamic process parameter changes (as described in Bui et al. (2014, 2018b)).

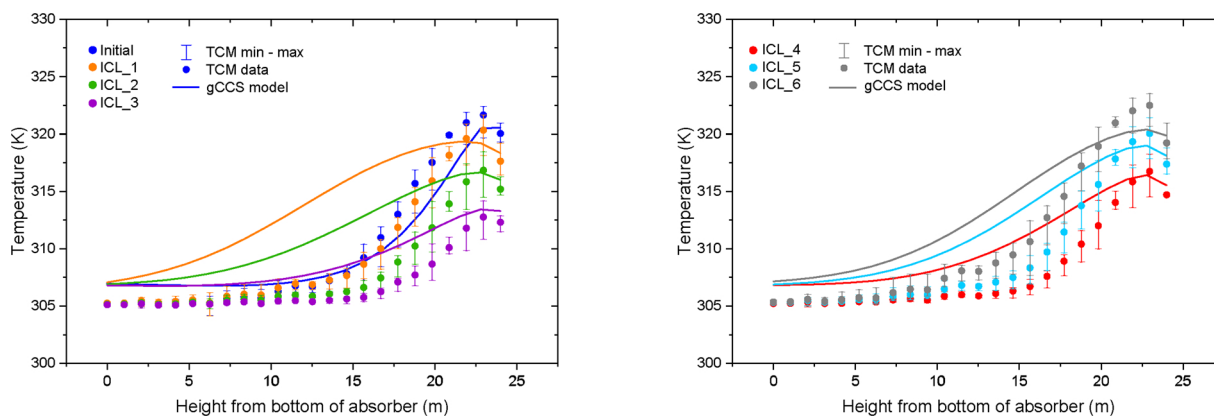


Fig. 11. Dynamic validation of the gCCS modelled absorber temperature against TCM plant data for the steam flow rate scenario. To prevent the overlapping of absorber temperature profiles, the data is separated into (left) initial to ICL₃, and (right) ICL₄ to ICL₆. Average absolute deviation between the TCM data and gCCS predictions for absorber temperature varies between 1.4 and 4.3 K (calculated in Table C.13).

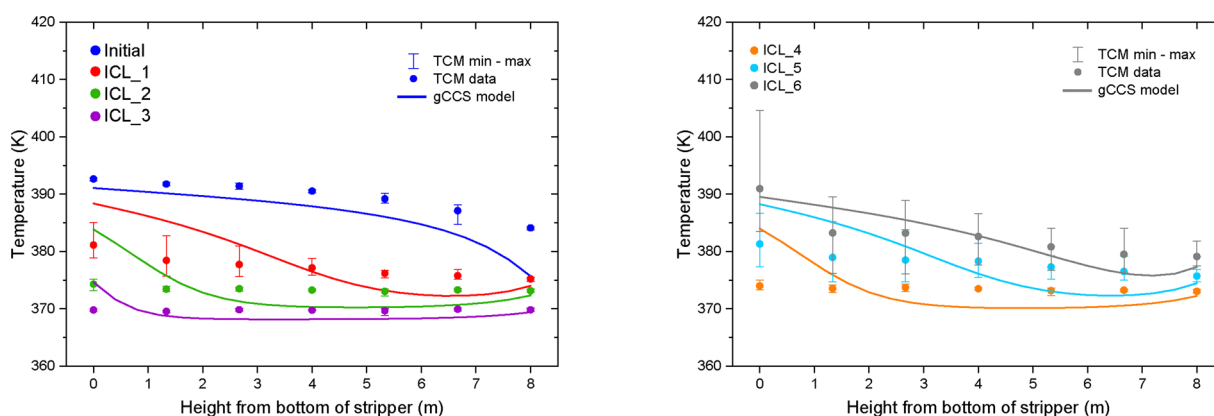


Fig. 12. Dynamic validation of the gCCS modelled stripper temperature against TCM plant data for the steam flow rate scenario. The data is separated into (left) initial to ICL₃, and (right) ICL₄ to ICL₆. Average absolute deviation between the TCM data and gCCS predictions for stripper temperature profiles varies between 1.7 and 3.7 K (calculated in Table C.13).

The off-peak mode (ICL₇ and ICL₉) simulated periods of reduced power generation, i.e., low electricity demand, which would allow the capture plant to ramp up solvent regeneration. To achieve this at the TCM plant, steam flow rate was increased to the upper limit of 5000 kg/h, flue gas flow rate was decreased (due to power output decrease) and solvent flow rate was reduced proportionally to maintain optimal L/G ratio (Fig. 2). Subsequently, the lean CO₂ loading decreased to 0.16 mol_{CO₂}/mol_{MEA}, which increased the CO₂ capture rate up to 89–97% and CO₂ product flow rate to 2600–2700 kg/h.

Conversely, in peak mode (ICL₈), the CO₂ was “stored” in the solvent by lowering steam flow rate to the minimum of 1000 kg/h and increasing the flows of flue gas and solvent. As a result, the CO₂ capture rate reduced to 14.5% and lean CO₂ loading increased to 0.48 mol_{CO₂}/mol_{MEA}. The observed relationship between the degree of capture and lean CO₂ loading concurs with findings from earlier modelling work by Mac Dowell and Shah (2015) and Mechleri et al. (2017). As operation switched between off-peak mode and peak mode, the rich CO₂ loading remained relatively constant at 0.52–0.53 mol_{CO₂}/mol_{MEA}. Similarly, the reboiler duty across the different operation modes were similar. The reboiler duty in off-peak mode ranged between 4.10 and 4.20 MJ/kg CO₂, whereas in peak mode, reboiler duty was around 4.49 MJ/kg CO₂.

Fig. 14 demonstrates the definite shift in capture performance as operation transitions from off-peak mode to peak mode. The off-peak mode absorbed more CO₂, thus the two absorber temperature profile are in regions of higher temperature with the temperature bulge at the top of the column. In contrast, due to the reduced heat supply to the stripper and increased flue gas flow, the peak mode captured very little CO₂. Consequently, the peak mode absorber profile was much lower in temperature

(almost horizontal) with no obvious temperature bulge. The model predictions of absorber column temperature is in good agreement with the TCM experimental data, evidenced by the low APD of 0.4–0.9%. The stripper temperature was challenging to model due to the gCCS software limitation of reboiler temperature window of operation. The model was unable to solve with low reboiler temperatures as this is outside the window of operation in gCCS.¹⁰ This temperature limit can be observed in Fig. 13, where gCCS seems to reach the minimal feasible CO₂ capture rate of 2.6%, thus is unable to simulate reboiler temperature < 115.8 °C. Consequently, using a reboiler temperature that was feasible within gCCS at the assumed process condition (i.e., 115.8 °C), resulted in the base temperature of the stripper temperature profile being poorly predicted. Similarly, the gCCS prediction of instantaneous CO₂ capture rate deviates from the TCM data (Fig. 13).

During the TCM experimental tests, process parameters were adjusted as single step changes, immediately changing flow settings to the new set-point values. The step change approach was employed for parameter changes in the dynamic model simulation of the time-varying solvent regeneration scenario. However, after the step change,

¹⁰ The CO₂ capture model library in gCCS has been validated using the pilot plant data from Tontiwachwuthikul et al. (1992) (published in Brand et al. (2012), Brand (2013)) and pilot plant studies by PSE; gCCS manual does not provide further detail. The operating range of the gCCS sub-models would likely be limited to the operating range of the calibration data used by the software developers. Consequently, this is the likely reason for convergence problems outside specific operating windows of certain sub-models, e.g., reboiler.

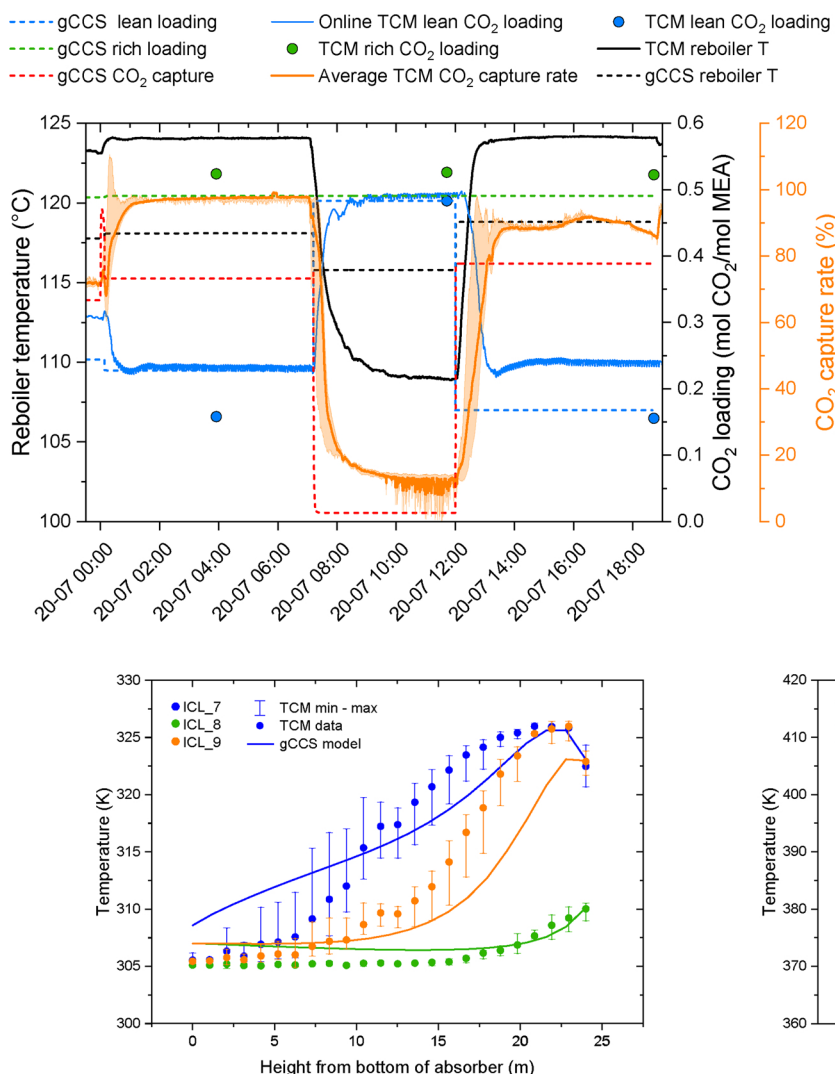


Fig. 13. The time-varying solvent regeneration scenario – the gCCS model results (dotted lines) in comparison with TCM process measurements (solid lines and points). There are four calculation methods for TCM CO₂ capture rate, the solid orange line shows the average TCM CO₂ capture rate and the shaded orange region illustrates the variance between the minimum and maximum values.

Fig. 14. Dynamic validation of the gCCS modelled temperature in the absorber (left) and stripper (right) against TCM plant data for the time-varying solvent scenario (ICL₇ to ICL₉). Average absolute deviation varies between 1.1 and 2.7 K for the absorber profiles and 6.3–7.4 K for the stripper (calculated in Table C.13).

the plant requires a duration of time to reach the final set-point (i.e., transition time), as well as further time to stabilise and reach steady state (i.e., stabilisation time). This time varies for different process parameters and with the magnitude of change, seen in Table C.14. Typically, larger step changes of process parameters require more time to reach the set-point value. However, these observed dynamics (e.g., solvent circulation time,¹¹ transition time, stabilisation time) are a function of the equipment design, i.e., archetype, construction material and dimensions. Solvent flow rate changes generally require more time for liquid redistribution compared to flue gas flow rate changes (Bui et al., 2016a). Solvent flow rate changes of higher magnitude impose a larger process disturbance, needing a greater amount of time for liquid redistribution. The dynamics of solvent and gas flow depend on column dimensions and type of internals (e.g., packing type, number and positioning of the liquid distributors). After steam flow rate changes, heat transfer effects will dictate the time to reach the final reboiler temperature. The dynamics of heat transfer during steam flow rate changes are a function of the reboiler design (thermosiphon heat exchanger) and fluid mechanics of the 2-phase system (vapour-liquid).

¹¹ The solvent circulation time (through the entire plant) is a function of lean/rich solvent flow rates and total liquid volume capacity of all the equipment/components.

Due to the large solvent inventory of 40.7–40.8 m³ at the TCM plant, the solvent circulation time is as long as 40–70 min, depending on the solvent flow rate (Montañés et al., 2018).¹² Hence, the observed changes to reboiler temperature, lean loading and CO₂ capture rate are gradual. In contrast, as a consequence of implementing lean loading changes as step changes, the modelled TCM process shows an immediate change in CO₂ capture rate, resulting in an inadequate description of the process transition from one time period to the next (i.e., ICL₇ to ICL₈); Fig. 13 shows this discrepancy. This highlights the importance of taking into account effects of solvent distribution and circulation time on the process dynamics when modelling flexible operation scenarios. Although the transition periods were inaccurately modelled, the model predicted the overall trends and the APD was ≤ 10% for most process variables at steady state periods (Tables C.12 and C.13).

The high lean CO₂ loading during peak mode of the time-varying solvent regeneration strategy indicates there was “storage” of CO₂ within the solvent. To quantify the storage capacity of the solvent, the cumulative CO₂ capture rate and amount of stored CO₂ was calculated to understand the effect on overall capture performance (presented in

¹² Previous tests demonstrate operation of the TCM capture plant with MEA solvent inventories as low as 38.2 m³ (Montañés et al., 2017) and high as 50 m³ (Flø et al., 2017).

Appendix C.5). Table C.15 indicates that the cumulative CO₂ capture rate of the first off-peak time period (ICL₇) was 95.5%, where 2022 kg of CO₂ was being stored in the solvent by the end of that time period. In contrast, the peak mode time period (ICL₈) had a cumulative capture rate of 20.5% but the amount of stored CO₂ increased significantly to 3668 kg of CO₂. The final off-peak mode (ICL₉) cumulatively captured 81.9%; where increased solvent desorption reduced the stored CO₂ to 2402 kg. Overall, the time-varying solvent regeneration scenario had a cumulative CO₂ capture rate of 66.5%, as shown in Table C.16. However, in this study, the duration of the time periods were not optimised to maximise cumulative CO₂ capture. Instead, time periods of 3–5 h were used to ensure the plant would reach steady state before the next process transition. Therefore, it is recommended that future design of an operating regime/schedule for the time-varying solvent regeneration strategy should consider process optimisation to ensure an appropriate cumulative CO₂ capture rate is achieved. This would involve co-ordinating the duration and capture performance of the off-peak mode and peak mode to meet a target cumulative CO₂ capture rate (e.g., cumulatively capture at least 90% of the CO₂).

5.3. Variable ramp rate

The power plant may be required to ramp up and down due to changes in electricity demand. As the power plant load varies, the flue gas flow rate will vary. Thus, a CO₂ capture plant that could ramp up and down in response to changes in power plant output could be advantageous, particularly for reducing residual emissions. Thus, the variable ramp rate scenario was designed to demonstrate capture plant flexibility in terms of ramping capabilities and limits. CCGT power plants typically can achieve ramp rates of 2–8%P_N/min, whereas gas turbines can ramp 8–15%P_N/min (Hentschel et al., 2016). However, at the time of this test campaign, the TCM CO₂ capture plant was using a process control system that was designed for steady state operation. Consequently, this process control system limited the maximum ramp rate of the TCM plant to 0.6% per min (i.e., % of the maximum flue gas flow and solvent flow). To increase the ramp rate of the TCM plant further, manual operation of the flue gas blower enabled a higher ramp rate of 1.7% per min and 5% per min. The TCM plant could potentially achieve faster ramp rates with a process control system designed for dynamic operation. As demonstrated in a separate study, flue gas flow ramp rates as high as 10% per min was achievable at TCM with decentralised control structures (Montañés et al., 2018).

In the variable ramp rate scenario, the flow rates of the flue gas, solvent and steam streams were changed simultaneously (ICL₁₀ to ICL₁₃ in Fig. 2). For each given ramp rate, the flue gas and solvent flow rates were ramped concurrently. However, the steam flow rate was controlled by a pressure valve, thus, progressively ramping steam flow was not possible. The steam flow rate change was implemented as a single step change. The L/G ratio was kept constant by ensuring the flue gas and solvent stream flows were ramped at the same rate. The ICL₁₀ and ICL₁₁ time periods employed a ramp rate of 0.6% per min decrease, whereas ICL₁₂ ramped up at 1.7% per min, and ICL₁₃ ramped up at 5% per min. As L/G ratio is constant, the lean and rich CO₂ loading remained relatively constant, shown in Fig. 15. Although different ramp rates were imposed on the process, the lean CO₂ loading remained reasonably constant between 0.14 and 0.16 mol_{CO₂}/mol_{MEA} and CO₂ capture rate was 87–89%. The rich CO₂ loading was also constant at ~0.53 mol_{CO₂}/mol_{MEA}. The dynamic model simulation of the variable ramp rate scenario also showed that CO₂ capture rate and lean/rich loading remained constant, with predicted values being in good agreement with the TCM plant data (APD values in Table C.12).

Fig. 6 illustrates the change in reboiler duty across the different time periods. It is a function of the reboiler heating rate and the CO₂ flow rate. Thus, as process parameters (steam, flue gas and solvent flow rates) were ramped down, the reboiler duty increased on a MJ per kg CO₂ basis. In contrast, ramping the flue gas, solvent and steam flow rates upward, reduced the reboiler duty from 4.28 to 4.36 MJ/kg CO₂

(ICL₁₁) to 4.08–4.10 MJ/kg CO₂ (ICL₁₃). The model predictions of reboiler duty were also in good agreement with the TCM data, with APD of predictions ranging between 2.6% and 11.4%.

Although the tested ramp rates (0.6–5% per min) are slightly conservative compared to typical CCGT ramp rates, this study demonstrates that different ramp rates can be applied to a capture plant in succession. By maintaining a constant L/G ratio throughout each ramp, the CO₂ capture performance remained constant, i.e., same CO₂ capture rate and solvent loading. Therefore, both the pilot plant and modelled results in Fig. 16 show that the absorber profile maintains the same temperature after every process ramp. Despite the changes to steam flow rate in this scenario, the TCM measurements showed little change to the reboiler temperature (Fig. 15). As this TCM reboiler temperature was used as an input for the gCCS model, the TCM and modelled stripper temperature profile appears to be almost constant after each ramp was implemented. Despite the use of variable ramp rates, a relatively high cumulative CO₂ capture rate of 88.2% was achieved with this scenario (Table C.16).

6. Conclusion

This study demonstrated that flexible operation is technically feasible in a large-scale CO₂ capture process using MEA solvent. The experimental study of three flexible operation scenarios (effect of steam flow rate, time-varying solvent regeneration and variable ramp rate) has provided invaluable insight into the dynamics of a CO₂ capture plant. The effect of steam flow rate on the performance of the process was established. As the steam flow rate decreased, there was an increase in lean CO₂ loading and a subsequent reduction in the CO₂ capture rate. Conversely, higher steam flow rate resulted in lower lean CO₂ loading and greater CO₂ capture rate. The time-varying solvent regeneration scenario was successfully demonstrated at the TCM CO₂ capture plant. In “off-peak” mode, the CO₂ capture rate increased up to 89–97%, whilst lean CO₂ loading reduced to 0.16 mol_{CO₂}/mol_{MEA} and CO₂ product flow rate was 2600–2700 kg/h. The “peak” mode of operation demonstrated that CO₂ could be stored in the solvent, where the stored amount of CO₂ almost doubled compared to off-peak mode. In peak mode, the CO₂ capture rate was lowered to 14.5% and lean CO₂ loading increased up to 0.48 mol_{CO₂}/mol_{MEA}. The variable ramp rate scenario demonstrated that different ramp rates could be applied successively to a CO₂ capture plant. By maintaining constant L/G ratio during the changes, the CO₂ capture performance remained the same (lean CO₂ loading of between 0.14 and 0.16 mol_{CO₂}/mol_{MEA} and CO₂ capture rate of 87–89%).

This flexible operation test campaign has provided useful operating experience in dynamic operation of a CO₂ capture facility. During the design of the test scenarios in collaboration with TCM, several key plant characteristics were found to limit the flexibility of the CO₂ capture plant, these include:

- **Stabilisation time:** There is a need to allow sufficient plant stabilisation time before changing to new process conditions. For test purposes, the TCM capture plant typically requires a minimum of 3 hours to stabilise and run at steady state before new process conditions can be implemented. This enables sufficient time to circulate and mix the solvent, ensuring representative solvent samples with homogeneous lean and rich solvent composition. However, the operation of a commercial plant would shorten the required stabilisation time as much as possible.
- **Transition time:** Step changes or rapid ramp rates to new set-point conditions do not occur immediately, and will differ from the actual transition time. The time to reach the final set-point conditions (i.e., transition time) depends on the process parameter and the magnitude of the parameter change (e.g., TCM specific times are provided in Table C.14).
- **Magnitude and speed of process parameter change:** Rapid and large process parameter changes tend to be avoided at TCM, e.g., flue gas flow rate change from 60,000 to 30,000 Sm³/h. These often

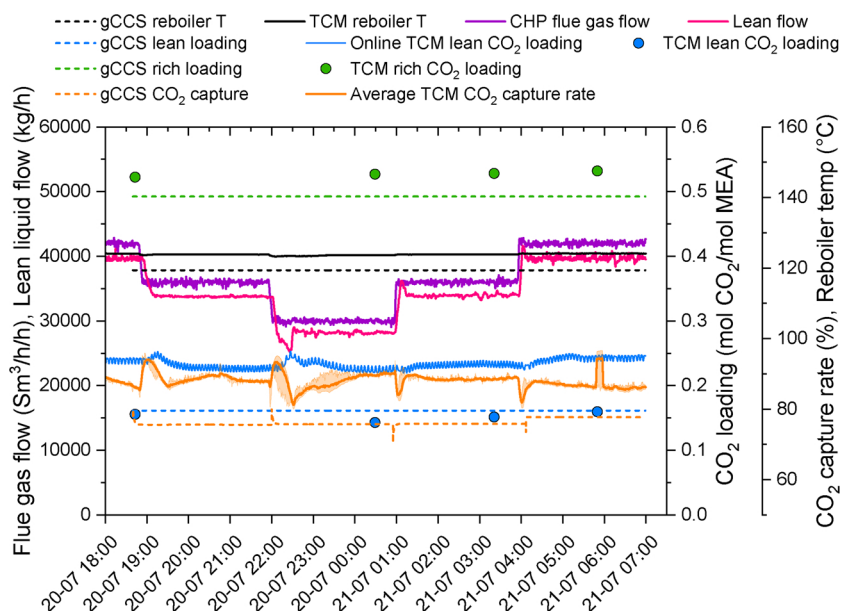


Fig. 15. The variable ramp rate scenario – the gCCS model results (dotted line) in comparison with TCM process measurements (solid line and points). The flue gas flow rate (blue line) and the lean solvent flow rate (pink line) are ramped simultaneously. Despite the step-changes to the steam flow rate, the reboiler temperature is almost constant. There are four calculation methods for TCM CO₂ capture rate, the solid orange line shows the average TCM CO₂ capture rate and the shaded orange region illustrates the variance between the minimum and maximum values. (For interpretation of the references to colour in this figure legend, the reader is referred to the web version of this article.)

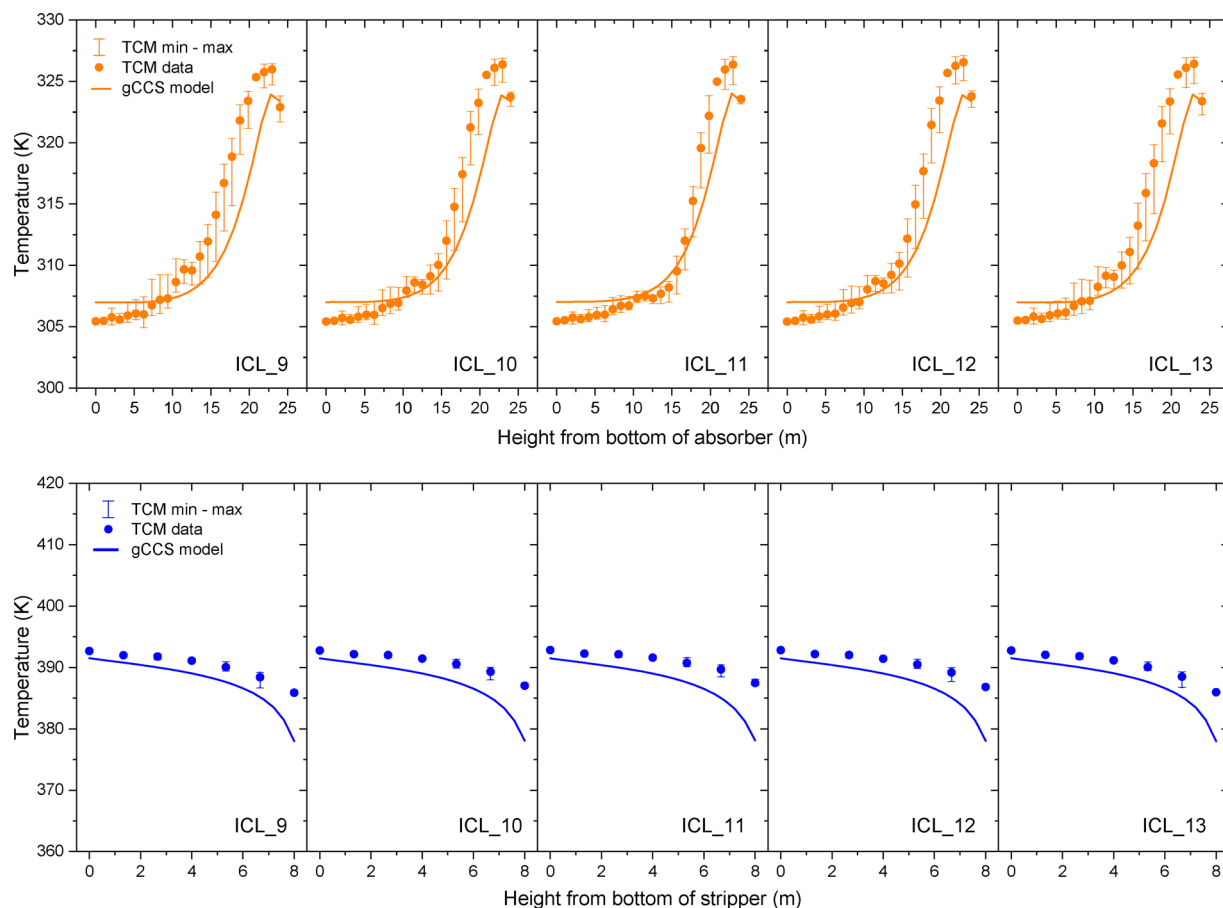


Fig. 16. Dynamic validation of the gCCS modelled temperature in the absorber (top) and stripper (bottom) against TCM plant data for the variable ramp rate scenario (ICL_9 to ICL_13). Average absolute deviation varies between 1.7 and 2.7 K for the absorber profiles and 3.8–6.3 K for the stripper (calculated in Table C.13).

lead to inverse responses and plant instability, which could take hours to stabilise. Typically, operators limit process parameter changes to $\sim 20\%$ of the maximum.

- **Process control system:** The process control system is designed for steady state operation. Consequently, this was found to be the key factor that limited the ramping capabilities of the TCM capture plant.

Furthermore, controller parameters, i.e., aggressive tuning compared with conservative tuning, will have a major influence on the stabilisation time, transition time and min-max operating window of the plant.

These were essential considerations in the design of the flexible operation test campaign at TCM to ensure stable plant operation and

efficient use of test time. The process control system in particular, limited the flexibility of the plant, e.g., limited ramp rates and required long stabilisation times. This study highlights the importance of having a process control system that is optimised for dynamic operation, which could potentially provide significant improvements to plant flexibility. Work is currently underway towards developing a dynamic process control system for the TCM testing facility, reported in another contribution (Montañés et al., 2018).

There has been significant progress in the area of dynamic and flexible operation of CO₂ liquid absorption processes. This study has shown that existing dynamic flowsheet modelling software still needs further improvement. There is deviation between the dynamic modelling results and experimental results from the TCM plant. Other contributions have also reported deviation between dynamic modelling results and pilot plant data using other commercial software to model: the Separation Research Program pilot plant in the United States (gPROMS model) (Biliyok et al., 2012), Brindisi pilot plant in Italy (K-Spice software) (Enaasen et al., 2014), Gløshaugen (NTNU/SINTEF) pilot plant in Norway (MATLAB model) (Flø et al., 2015), TCM CO₂ capture plant (Gas Liquid Contactors library in Modelica) (Montañés et al., 2017) and a pilot plant built at the Maasvlakte power station in Netherlands (ThermalSeparation Modelica library) (van de Haar et al., 2017). Continual development in our understanding of the underlying processes and mechanisms of CO₂ absorption is essential, both from modelling and plant operation perspectives. As more pilot plant studies conduct dynamic and flexible operation testing, more dynamic experimental data will become available from different CO₂ capture facilities. Such data would provide invaluable insight into the effects of plant scale and plant topology on dynamic CO₂ capture performance. These insights and data should feed into software and model development to improve our ability to simulate flexible operation of CO₂ capture plants.

An important consideration for plant flexibility is the trade-off between CO₂ storage capacity and the volume of solvent inventory. On one hand, increasing the volume of solvent inventory could provide greater CO₂ storage capacity (advantageous for the time-varying solvent regeneration strategy). However, the larger solvent inventory would lead to slower dynamics, increasing the solvent circulation,

transition and stabilisation times for the CO₂ capture plant. Therefore, solvent development and design should focus on improving fluid flow properties and increasing the working capacity of solvents (Raksajati et al., 2013; Zhang et al., 2016; Bernhardsen and Knuutila, 2017), which could provide significant improvement to plant flexibility. Increasing solvent working capacity would be particularly useful for the time-varying solvent regeneration strategy as it enable more moles of CO₂ to be “stored” per mole of liquid absorbent.

In this work, the scenarios were designed based on the premise that the dynamics of the power plant is limited by the steam generation rate or combustion rate, e.g., in subcritical, supercritical, ultra-supercritical power plants (Miller, 2017; Alobaid et al., 2017). In combined cycle gas turbine (CCGT) power plants, approximately two-thirds of the total power output is generated by the gas turbine, whereas one-third is by the steam turbine (Seebregts, 2010). This suggests that the dynamic behaviour of the overall CCGT power output is potentially dictated mainly by the gas turbine, where the steam cycle has some influence on the dynamics but to a smaller extent, i.e., “gas turbine-limited” dynamics. Thus, it is possible that steam extraction for CO₂ capture from CCGT power plants, with “gas turbine-limited” dynamics, may have a negligible effect on the overall electricity output (i.e., no energy penalty). Further research is needed to study and identify the key process bottleneck that limit overall flexibility of the integrated power plant and CCS system, thereby enabling process improvement and design.

Conflict of interest

None declared.

Acknowledgements

We are grateful for the support of Technology Centre Mongstad (TCM) and TCM owners Gassnova, Equinor, Shell and Total in conducting this test campaign. The authors would like to also acknowledge funding from the Research Councils UK (RCUK) under grants EP/M001369/1 (MESMERISE-CCS), EP/M015351/1 (Opening New Fuels for UK Generation), EP/N024567/1 (CCSInSupply), and NE/P019900/1 (GGR Opt).

Appendix A. Specification of the TCM CO₂ capture plant

Table A.2

Column specifications of the absorber and CHP stripper at the TCM CO₂ capture pilot plant (Andersson et al., 2013; Hamborg et al., 2014; Montañés et al., 2017; Koch-Glitsch, 2010).

	Absorber	CHP stripper
Geometry	Rectangular	Cylindrical
Total height (m)	62	30
Cross sectional area (m ²)	3.55 m × 2 m	–
Diameter (m)	–	1.3
Packing type	Flexipac 2X structured	Flexipac 2X structured
Packing height (m)	24	8
Vendor	Koch Glitsch	Koch Glitsch
Material of packing	Stainless steel	Stainless steel
Surface area (m ² /m ³)	225	225
Void fraction	0.97	0.97
Sump volume (m ³)	8.1	2.3
	Absorber wash section	Stripper wash section
Packing height (m)	6	1.6
Packing type	Flexipac 2Y HC structured	Flexipac 2Y HC structured
Packing vendor	Koch Glitsch	Koch Glitsch
Material of packing	Stainless steel	Stainless steel
Full load capacity (t/h)	50 or 60	–
Reboiler type	–	Welded plate thermosiphon HX

Table A.3
Typical flue gas composition from the natural gas fired CHP plant
(Andersson et al., 2013).

Flue gas component	Composition (mol%)
N ₂	78.6
CO ₂	3.6
H ₂ O	2.5
O ₂	14.4
Ar	0.9

Appendix B. Calculation methods

B.1 Thermal energy requirements – specific reboiler duty

The specific reboiler duty is the reboiler heating rate (MJ/h) divided by the product CO₂ flow rate (kg/h). There are two methods to calculate this value (adapted from Hamborg et al. (2014), Faramarzi et al. (2017)):

1. **Method 1:** reboiler heating rate is divided by the measured CO₂ product flow rate.
2. **Method 2:** reboiler heating rate is divided by the difference between the measured CO₂ supply flow and the CO₂ flow in the depleted gas (this difference is equivalent to the CO₂ product flow rate).

The flow rates used to calculate the capture rate and reboiler duty presented in Fig. C.19.

B.2 CO₂ capture rate

The following table shows the calculation methods for CO₂ capture rate, i.e., CO₂ capture efficiency (adapted from Hamborg et al. (2014), Faramarzi et al. (2017)).

B.3 Degree of deviation calculation

Absolute deviation demonstrates the degree of deviation between the pilot plant data and model predictions as a percentage. The absolute percentage deviation (APD) is calculated as:

$$APD = 100 \times \left| \frac{X_m - X_p}{X_p} \right| \quad (B.1)$$

where X_m is the model prediction of a specific process parameter (e.g., lean CO₂ solvent loading, CO₂ capture rate, reboiler duty), and X_p is the pilot plant value. For each case/scenario, the APD values is calculated and presented in the tables. For absorber and stripper temperature profiles, the mean of all APD values along the height of the column is calculated and referred to as the average absolute percentage deviation (average APD) – this is calculated based on temperature units of kelvin (K).

Table B.4

Description of the four methods used to calculate the CO₂ capture rate.

CO ₂ capture efficiency	Description	Formula
Method 1	Ratio of the CO ₂ product flow to the CO ₂ flow in the flue gas supply	$= \frac{CO_2(\text{product})}{CO_2(\text{supply})}$
Method 2	Ratio of the CO ₂ product flow to the sum of the CO ₂ product flow and CO ₂ flow in the depleted flue gas	$= \frac{CO_2(\text{product})}{CO_2(\text{product}) + CO_2(\text{depleted})}$
Method 3	Ratio of the difference between the CO ₂ flow in the flue gas supply and the CO ₂ in the depleted flue gas to the CO ₂ flow in the flue gas supply	$= \frac{CO_2(\text{supply}) - CO_2(\text{depleted})}{CO_2(\text{supply})}$
Method 4	100% minus the ratio of the depleted flue gas CO ₂ per unit O ₂ + N ₂ to the flue gas supply CO ₂ per unit O ₂ + N ₂	$= 1 - \frac{O_{CO_2}(1 - I_{CO_2})}{(1 - O_{CO_2})I_{CO_2}}$ $O_{CO_2} = \text{CO}_2 \text{ content of depleted outflow flue gas}$ $I_{CO_2} = \text{dry basis CO}_2 \text{ content of input supply flue gas, dry basis}$

Appendix C. TCM CO₂ capture plant: datasets of results

C.1 Flexible operation test campaign schedule

Table C.5

The start date/time of each time period (ICL_1 to ICL_13) over the duration of the TCM flexible operation campaign. The “Initial” time period is the steady state conditions of the TCM plant just before flexible operation campaign commences. The start steady state and end steady state date/time is the period of data used to calculate the average steady state conditions in [Tables C.8–C.11](#).

Time period	[dd/mm/yyyy hh:mm]		
	Start scenario	Start steady state	End steady state
Initial	18/07/2017 22:00	19/07/2017 04:00	19/07/2017 04:59
ICL_1	19/07/2017 05:00	19/07/2017 05:59	19/07/2017 08:59
ICL_2	19/07/2017 09:00	19/07/2017 10:00	19/07/2017 11:59
ICL_3	19/07/2017 12:00	19/07/2017 13:00	19/07/2017 14:58
ICL_4	19/07/2017 15:00	19/07/2017 16:00	19/07/2017 17:59
ICL_5	19/07/2017 18:00	19/07/2017 19:00	19/07/2017 20:56
ICL_6	19/07/2017 21:00	19/07/2017 22:00	19/07/2017 23:58
ICL_7	20/07/2017 00:00	20/07/2017 01:00	20/07/2017 06:58
ICL_8	20/07/2017 07:00	20/07/2017 08:00	20/07/2017 11:58
ICL_9	20/07/2017 12:00	20/07/2017 13:00	20/07/2017 18:35
ICL_10	20/07/2017 18:40	20/07/2017 19:40	20/07/2017 21:57
ICL_11	20/07/2017 22:00	20/07/2017 23:00	21/07/2017 00:57
ICL_12	21/07/2017 01:00	21/07/2017 02:00	21/07/2017 03:56
ICL_13	21/07/2017 04:00	21/07/2017 05:00	21/07/2017 06:56

C.2 TCM plant results and gCCS model validation

Table C.6

Baseline process conditions used for steady state validation of the gCCS model (shown as absolute percentage deviation). The 2014 baseline data from [Hamborg et al. \(2014\)](#) and the 2015 baseline data is from [Faramarzi et al. \(2017\)](#). The S for volumetric gas flow rate units (Sm^3/h) denotes standard conditions of 1 atm and 15 °C.

Specification	2014 Baseline	2015 Baseline
Flue gas flow rate (Sm^3/h)	46,970	59,430
Lean solvent flow (kg/h)	54,900	57,434
L/G ratio (kg liq/ Sm^3 gas)	1.17	0.97
Feed flue gas CO_2 concentration (vol%)	3.7	3.7
Feed flue gas H_2O concentration (vol%)	2.5*	3.7
Absorber flue gas inlet temperature (°C)	25.0	29.8
Absorber solvent inlet temperature (°C)	36.5	37.0
Stripper solvent inlet temperature (°C)	108.6	110.7
Stripper overhead pressure (barg)	0.90	0.91
Reboiler temperature (°C)	122.3	125.1
MEA concentration (wt%)	30	30
Lean CO_2 loading ($\text{mol}_{\text{CO}_2}/\text{mol}_{\text{MEA}}$)	0.23	0.20
Rich CO_2 loading ($\text{mol}_{\text{CO}_2}/\text{mol}_{\text{MEA}}$)	0.48	0.48
TCM plant CO_2 capture rate (%)	93.5	83.4
TCM Reboiler duty (MJ/kg CO_2)	4.14	3.62
gCCS lean loading ($\text{mol}_{\text{CO}_2}/\text{mol}_{\text{MEA}}$)	0.2302	0.2317
APD lean loading (%)	0.07	15.9
gCCS rich loading ($\text{mol}_{\text{CO}_2}/\text{mol}_{\text{MEA}}$)	0.4985	0.4934
APD rich loading (%)	3.9	2.8
gCCS plant CO_2 capture rate (%)	94.7	80.1
APD capture rate (%)	1.3	4.0
References	Hamborg et al. (2014) * Flue gas water content from Andersson et al. (2013)	Faramarzi et al. (2017)

Table C.7

Absorber and stripper column temperature for the two steady state validation cases, where APD shows the degree of model deviation. The 2014 baseline data is from [Hamborg et al. \(2014\)](#) and the 2015 baseline data is from [Faramarzi et al. \(2017\)](#)

Packing height from ABS base (m)	2014 Baseline ABS temperature (°C)	2015 Baseline ABS temperature (°C)
0.00	27.2	32.4
1.04	27.6	32.5
2.09	28.4	33.2
3.13	28.1	32.9
4.17	29.3	33.8
5.22	29.8	34.1
6.26	30.4	34.3
7.30	32.2	35.9
8.35	33.7	37.1
9.39	35.0	37.4
10.43	39.1	41.6
11.48	38.4	40.6
12.52	39.0	40.9
13.57	40.6	42.2
14.61	41.7	43.1
15.65	43.5	44.4
16.70	45.2	46.0
17.74	46.7	47.2
18.78	48.5	48.9
19.83	49.6	49.9
20.87	50.3	50.5
21.91	51.2	51.6
22.96	51.1	51.7
24.00	45.4	47.4
Min-max absolute deviation (K)	0.6–7.2	0.7–5.3
Average absolute deviation (K)	3.1	2.9
Average APD (%)	0.98	0.94

Packing height from STR base (m)	STR temperature (°C)	STR temperature (°C)
0.00	–	119.4
1.33	–	114.7
2.67	–	112.1
4.00	–	107.7
5.33	–	104.5
6.67	–	103.1
8.00	–	102.7
Min-max absolute deviation (K)	–	0.7–3.7
Average absolute deviation (K)	–	2.3
Average APD (%)	–	0.59

Table C.8

Steady state process conditions for each time period from ICL_1 to ICL_13 over the course of the flexible operation campaign (refer to [Table C.5](#) for the actual date/time).

	Initial	ICL_1	ICL_2	ICL_3	ICL_4	ICL_5	ICL_6	ICL_7	ICL_8	ICL_9	ICL_10	ICL_11	ICL_12	ICL_13
Feed flue gas CO ₂ concentration, wet GC (vol%)	3.64	3.64	3.79	3.79	3.58	3.58	3.60	3.60	3.59	3.91	4.02	4.07	4.07	4.09
Feed flue gas O ₂ concentration, GC (vol%)	15.25	15.25	14.95	14.88	15.23	15.22	15.21	15.16	15.21	14.56	14.36	14.28	14.30	14.29
Feed flue gas H ₂ O concentration, GC (vol%)	4.457	4.464	4.497	4.489	4.478	4.491	4.468	4.565	4.501	4.562	4.584	4.615	4.594	4.579
Absorber flue gas inlet temp (°C)	29.93	29.97	30.05	30.14	30.15	30.11	30.05	30.06	30.13	30.21	30.16	30.11	30.08	30.08
CHP flue gas feed flow rate (Sm ³ /h)	60,536	60,522	60,509	60,527	60,569	60,621	60,567	41,873	60,554	41,964	35,951	29,907	35,842	41,776
MEA concentration (wt%)	27.5	–	26.2	25.8	–	27.0	27.3	27.9	25.5	27.8	–	27.8	27.4	28.0
Lean amine supply temp (°C)	37.00	37.00	37.00	37.01	37.00	37.01	37.01	37.00	36.99	37.01	37.01	36.98	36.98	37.02
Lean solvent flow rate (kg/h)	45,557	58,326	58,856	59,667	58,898	58,249	57,684	39,587	60,095	39,496	33,775	28,170	33,952	39,699
Rich solvent flow rate (kg/h)	48,824	60,816	60,799	60,822	60,793	60,797	60,797	42,561	60,789	42,428	36,465	30,402	36,519	42,561
L/G ratio (kg liquid/Sm ³ gas)	0.7526	0.9637	0.9727	0.9858	0.9724	0.9609	0.9524	0.9454	0.9924	0.9412	0.9395	0.9419	0.9473	0.9503
Steam flow rate (kg/h)	5234	4055	3013	1982	3001	4002	5032	5009	1098	5002	4542	3943	4519	5024
Rich solvent supply temp (°C)	110.96	102.06	99.98	96.67	99.90	102.55	105.97	112.94	92.05	112.73	113.87	114.31	113.66	112.81
Stripper bottom pressure (barg)	0.937	0.933	0.928	0.925	0.928	0.929	0.935	0.933	0.920	0.927	0.927	0.928	0.930	0.930
Reboiler solution temperature (°C)	124.16	121.89	119.50	115.19	119.57	121.82	123.25	124.06	109.54	124.10	123.84	123.61	123.86	124.13

Table C.9

Steady state lean CO₂ loading, rich CO₂ loading, capture rate (4 calculation methods) and reboiler duty (2 calculation method) for each time period from ICL₁ to ICL₁₃ over the course of the flexible operation campaign (refer to Table C.5 for the actual date/time). The laboratory could only analyse a limited number of solvent samples per day. Consequently, manual lean/rich loading measurements could not be carried out for all time periods, these appear as – in the results table.

TCM data	Initial	ICL ₁	ICL ₂	ICL ₃	ICL ₄	ICL ₅	ICL ₆	ICL ₇	ICL ₈	ICL ₉	ICL ₁₀	ICL ₁₁	ICL ₁₂	ICL ₁₃
Lean CO ₂ loading titration (mol _{CO₂} /mol _{MEA})	0.1691	–	0.3649	0.4375	–	0.2814	0.2456	0.1580	0.4830	0.1556	–	0.1428	0.1513	0.1596
Lean CO ₂ loading online (mol _{CO₂} /mol _{MEA})	0.2350	0.3434	0.3908	0.4440	0.4001	0.3535	0.3093	0.2321	0.4869	0.2383	0.2272	0.2271	0.2324	0.2435
Rich CO ₂ loading (mol _{CO₂} /mol _{MEA})	0.5176	–	0.5315	–	–	0.5217	–	0.5237	0.5261	0.5225	–	0.5270	0.5282	0.5321
CO ₂ capture rate Method 1 (%)	75.02	59.98	41.92	25.83	44.54	59.35	72.90	96.64	12.34	90.06	88.60	89.87	88.67	86.66
CO ₂ capture rate Method 2 (%)	73.38	59.65	42.01	26.14	44.07	58.99	72.29	97.52	12.59	88.78	88.68	88.54	88.69	87.22
CO ₂ capture rate Method 3 (%)	72.78	59.43	42.14	27.03	43.46	58.74	72.06	97.54	15.43	88.51	88.69	88.34	88.69	87.21
CO ₂ capture rate Method 4 (%)	72.34	58.78	41.11	25.74	42.62	58.13	71.65	97.50	14.23	88.30	88.48	88.11	88.47	86.96
TCM CO ₂ capture rate average (%)	73.02	59.14	41.47	25.95	43.28	58.49	71.96	97.32	13.68	88.70	88.50	88.50	88.51	86.91
Reboiler duty (MJ/kg CO ₂) Meth1	3.92	3.74	3.81	4.11	3.79	3.77	3.90	4.20	12.30	4.10	4.27	4.28	4.20	4.10
Reboiler duty (MJ/kg CO ₂) Meth2	4.04	3.77	3.80	3.93	3.89	3.80	3.94	4.16	4.49	4.18	4.26	4.36	4.20	4.08

Table C.10

Steady state absorber mean temperature for each time period from ICL₁ to ICL₁₃ over the course of the flexible operation campaign (refer to Table C.5 for the actual date/time). The data for the four temperature probes (A, B, C and D) at each height is provided in the Supplementary Material; this data is used to generate the min-max error bars on the temperature profile.

Packing height from ABS base (m)	Absorber column temperature (°C)													
	Initial	ICL ₁	ICL ₂	ICL ₃	ICL ₄	ICL ₅	ICL ₆	ICL ₇	ICL ₈	ICL ₉	ICL ₁₀	ICL ₁₁	ICL ₁₂	ICL ₁₃
0.00	32.07	32.09	31.99	31.95	32.06	32.15	32.19	32.39	31.96	32.28	32.27	32.29	32.27	32.34
1.04	32.09	32.10	32.00	31.95	32.07	32.17	32.21	32.42	31.96	32.33	32.33	32.36	32.33	32.39
2.09	32.22	32.29	32.13	32.04	32.18	32.32	32.42	33.17	32.03	32.62	32.57	32.60	32.59	32.67
3.13	32.09	32.13	31.99	31.92	32.05	32.18	32.25	32.74	31.91	32.43	32.41	32.46	32.42	32.48
4.17	32.13	32.23	32.03	31.91	32.08	32.26	32.41	33.77	31.89	32.75	32.66	32.64	32.68	32.77
5.22	32.28	32.37	32.17	32.05	32.22	32.41	32.57	33.96	32.01	32.92	32.82	32.81	32.84	32.93
6.26	32.02	32.12	32.07	32.00	32.18	32.40	32.55	34.41	31.95	32.85	32.81	32.82	32.92	33.01
7.30	32.50	32.68	32.34	32.14	32.37	32.67	33.01	35.99	32.06	33.58	33.36	33.26	33.40	33.52
8.35	32.65	32.87	32.45	32.21	32.48	32.85	33.30	37.70	32.10	34.03	33.72	33.55	33.77	33.91
9.39	32.56	32.80	32.34	32.06	32.35	32.80	33.26	38.86	31.93	34.15	33.78	33.57	33.85	33.95
10.43	33.12	33.43	32.68	32.28	32.70	33.33	34.27	42.20	32.11	35.50	34.80	34.19	34.88	35.10
11.48	33.59	33.80	32.81	32.31	32.82	33.65	34.92	44.08	32.13	36.52	35.45	34.36	35.55	36.00
12.52	33.52	33.71	32.71	32.22	32.73	33.56	34.86	44.23	32.06	36.43	35.28	34.16	35.38	35.91
13.57	34.06	34.11	32.89	32.33	32.93	33.94	35.60	46.19	32.12	37.57	35.96	34.53	36.07	36.84
14.61	34.67	34.50	33.09	32.46	33.14	34.33	36.31	47.55	32.20	38.80	36.88	35.04	36.99	37.93
15.65	36.06	35.48	33.45	32.59	33.54	35.16	37.45	49.00	32.24	40.97	38.86	36.37	39.02	40.08
16.70	37.80	36.84	34.29	33.10	34.42	36.56	39.54	50.32	32.54	43.55	41.62	38.86	41.82	42.74
17.74	39.84	38.69	35.68	33.94	35.76	38.29	41.41	51.00	33.01	45.71	44.27	42.10	44.53	45.17
18.78	42.53	40.93	37.07	34.54	37.24	40.59	44.05	51.86	33.24	48.65	48.09	46.41	48.30	48.42
19.83	44.38	42.76	38.66	35.50	38.84	42.45	45.78	52.25	33.72	50.25	50.10	49.03	50.29	50.21
20.87	46.74	44.99	40.76	36.94	40.87	44.66	47.82	52.84	34.50	52.19	52.37	51.83	52.53	52.41
21.91	47.83	46.44	42.68	38.63	42.68	46.17	48.86	52.80	35.43	52.60	52.95	52.82	53.12	52.96
22.96	48.51	47.17	43.68	39.60	43.58	46.89	49.33	52.69	36.07	52.83	53.23	53.21	53.40	53.27
24.00	46.89	44.47	42.02	39.15	41.53	44.22	46.06	49.33	36.88	49.74	50.58	50.41	50.63	50.23

Table C.11

Steady state stripper mean temperature for each time period from ICL₁ to ICL₁₃ over the course of the flexible operation campaign (refer to Table C.5 for the actual date/time). The data for the four temperature probes (A, B, C and D) at each height is provided in the Supplementary Material; this data is used to generate the min-max error bars on the temperature profile.

Packing height from stripper base (m)	Stripper column temperature (°C)													
	Initial	ICL ₁	ICL ₂	ICL ₃	ICL ₄	ICL ₅	ICL ₆	ICL ₇	ICL ₈	ICL ₉	ICL ₁₀	ICL ₁₁	ICL ₁₂	ICL ₁₃
0.00	119.46	107.98	101.15	96.63	100.84	112.68	117.81	125.64	98.08	125.79	125.85	125.82	125.77	125.71
1.33	118.60	105.30	100.28	96.40	100.37	105.82	110.08	118.93	91.80	118.83	119.00	119.10	119.02	118.90
2.67	118.26	104.57	100.35	96.69	100.56	105.34	110.04	118.71	92.10	118.62	118.87	118.99	118.87	118.66
4.00	117.39	103.98	100.11	96.60	100.34	105.16	109.46	118.01	92.01	117.94	118.28	118.44	118.26	118.00
5.33	116.02	103.02	99.90	96.50	100.01	104.15	107.65	116.94	91.91	116.88	117.39	117.60	117.32	116.91
6.67	113.95	102.63	100.15	96.79	100.11	103.36	106.36	115.42	92.21	115.25	116.15	116.51	116.01	115.34
8.00	110.96	102.06	99.98	96.67	99.90	102.55	105.97	112.94	92.05	112.73	113.87	114.31	113.66	112.81

Table C.12

The absolute percentage deviation (APD) of the gCCS model results is calculated for each time period (ICL_1 to ICL_13) during the TCM test campaign. The process parameters compared include lean and rich loading, average CO₂ capture rate and reboiler duty (2 calculation methods). Refer to Table C.5 for the actual date/time. The titration lean loading measurements for ICL_1 and ICL_4 are not available (Table C.8). The lean loading from the period operating at the same process conditions is used for model validation purposes: * uses ICL_5 lean loading for model validation, # uses the lean loading from ICL_2 results. Online lean loading is not calibrated for this campaign solvent, thus there is a large APD (refer to section 3.4 for explanation).

	Initial	ICL_1	ICL_2	ICL_3	ICL_4	ICL_5	ICL_6	ICL_7	ICL_8	ICL_9	ICL_10	ICL_11	ICL_12	ICL_13
TCM online lean loading (molCO ₂ /mol _{MEA})	0.2350	0.3434	0.3908	0.4440	0.4001	0.3535	0.3093	0.2321	0.4869	0.2383	0.2272	0.2271	0.2324	0.2435
gCCS lean loading (molCO ₂ /mol _{MEA})	0.1855	0.2707	0.3271	0.3856	0.3259	0.2729	0.2441	0.2316	0.4830	0.1679	0.1613	0.1613	0.1614	0.1613
APD lean loading (%)	21.07	21.16	16.28	13.15	18.55	22.79	21.08	0.22	0.81	29.57	29.00	28.98	30.57	33.76
TCM lean CO ₂ loading (molCO ₂ /mol _{MEA})	0.1691	0.2814*	0.3649	0.4375	0.3649#	0.2814	0.2456	0.1580	0.4830	0.1556		0.1428	0.1513	0.1596
gCCS lean loading (molCO ₂ /mol _{MEA})	0.1855	0.2707	0.3271	0.3856	0.3259	0.2729	0.2441	0.2316	0.4830	0.1679	0.1613	0.1613	0.1614	0.1613
APD lean loading (%)	9.69	3.79	10.35	11.85	10.69	3.01	0.63	46.59	0.01	7.90		12.94	6.62	1.07
TCM rich CO ₂ loading (molCO ₂ /mol _{MEA})	0.5176		0.5315			0.5217		0.5237	0.5261	0.5225		0.5270	0.5282	0.5321
gCCS rich loading (molCO ₂ /mol _{MEA})	0.4910	0.4868	0.4894	0.4375	0.4905	0.4898	0.4885	0.4881	0.4907	0.4908	0.4925	0.4925	0.4925	0.4925
APD rich loading (%)	5.13		7.92			6.12		6.80	6.73	6.07		6.55	6.75	7.44
TCM CO ₂ capture rate (%)	73.02	59.14	41.47	25.95	43.28	58.49	71.96	97.32	13.68	88.70	88.50	88.50	88.51	86.91
gCCS CO ₂ capture rate (%)	68.78	59.83	44.49	27.98	44.18	58.69	66.70	86.81	2.62	77.71	75.57	75.72	75.81	77.71
APD CO ₂ capture rate (%)	5.82	1.17	7.28	7.82	2.08	0.35	7.30	10.80	80.82	12.39	14.60	14.45	14.35	10.58
TCM reboiler duty (MJ/kg CO ₂) Meth 1	3.92	3.74	3.81	4.11	3.79	3.77	3.90	4.20	12.30	4.10	4.27	4.28	4.20	4.10
gCCS reboiler duty (MJ/kg CO ₂)	3.97	3.55	3.80	4.33	3.78	3.50	3.46	3.68	3.91	4.38	4.50	4.47	4.50	4.54
APD reboiler duty (%)	1.35	4.94	0.44	5.31	0.23	6.93	11.20	12.32	68.21	6.80	5.38	4.43	7.15	10.77
TCM reboiler duty (MJ/kg CO ₂) Meth 2	4.04	3.77	3.80	3.93	3.89	3.80	3.94	4.16	4.49	4.18	4.26	4.36	4.20	4.08
gCCS reboiler duty (MJ/kg CO ₂)	3.97	3.55	3.80	4.33	3.78	3.50	3.46	3.68	3.91	4.38	4.50	4.47	4.50	4.54
APD reboiler duty (%)	1.67	5.83	0.07	10.18	2.71	7.87	12.22	11.50	12.95	4.75	5.49	2.63	7.19	11.37

Table C.13

The deviation between the gCCS model and TCM mean temperature data for the steady state absorber and stripper temperature profiles for each time period (ICL_1 to ICL_13) over the course of the flexible operation campaign (refer to Table C.5 for the actual date/time). Deviation is expressed as absolute deviation (K) and absolute percentage deviation (%).

	Initial	ICL_1	ICL_2	ICL_3	ICL_4	ICL_5	ICL_6	ICL_7	ICL_8	ICL_9	ICL_10	ICL_11	ICL_12	ICL_13
ABS T profile														
Min absolute deviation (K)	0.34	0.29	0.26	0.65	0.31	0.51	0.31	0.34	0.08	0.07	0.30	0.16	0.26	0.03
Max absolute deviation (K)	3.30	8.31	6.24	3.36	4.63	5.58	5.32	5.05	1.91	7.53	6.74	5.38	6.89	7.04
Average absolute deviation (K)	1.41	4.27	3.25	2.09	2.41	2.73	2.82	2.72	1.12	2.67	2.11	1.67	2.16	2.32
Average APD (%)	0.45	1.39	1.06	0.68	0.78	0.89	0.91	0.87	0.37	0.84	0.66	0.53	0.68	0.73
STR T profile														
Min absolute deviation (K)	1.54	0.65	0.80	0.43	0.81	1.25	0.49	2.81	0.03	3.16	1.40	1.50	1.42	1.27
Max absolute deviation (K)	8.41	7.23	9.54	4.84	9.99	6.12	4.19	9.08	17.22	9.49	8.97	9.37	8.76	7.99
Average absolute deviation (K)	3.43	3.71	3.31	1.73	3.52	3.25	2.28	6.34	7.35	6.29	4.22	4.42	4.15	3.76
Average APD (%)	0.88	0.98	0.89	0.47	0.94	0.86	0.60	1.62	2.00	1.61	1.08	1.13	1.06	0.96

C.3 TCM plant transition times

Table C.14

Time (min) to reach the set-point value after step changes and ramps of the key process parameters, *i.e.*, transition time from one set of conditions to the new set of conditions (e.g., from time period ICL_1 to ICL_2). The steam flow rate is controlled by a pressure valve, thus, progressively ramping steam flow is not possible. The steam flow rate change was implemented as a single step change and the table indicates the time it takes for the reboiler to reach the final temperature value.

Transition	Time to reach set-point value (minutes)		
	Flue gas flow rate	Solvent flow rate	Reboiler temperature
Initial → ICL_1	–	–	55
ICL_1 → ICL_2	–	–	20
ICL_2 → ICL_3	–	–	100
ICL_3 → ICL_4	–	–	75
ICL_4 → ICL_5	–	–	40
ICL_5 → ICL_6	–	–	30
ICL_6 → ICL_7	25	19	15
ICL_7 → ICL_8	41	43	114

(continued on next page)

Table C.14 (continued)

Transition	Time to reach set-point value (minutes)		
	Flue gas flow rate	Solvent flow rate	Reboiler temperature
ICL_8 → ICL_9	32	88	40
ICL_9 → ICL_10	32	37	26
ICL_10 → ICL_11	5	5	5
ICL_11 → ICL_12	4	4	4
ICL_12 → ICL_13	8	8	8

C.4 Effect of steam flow rate on the reboiler temperature during flexible operation

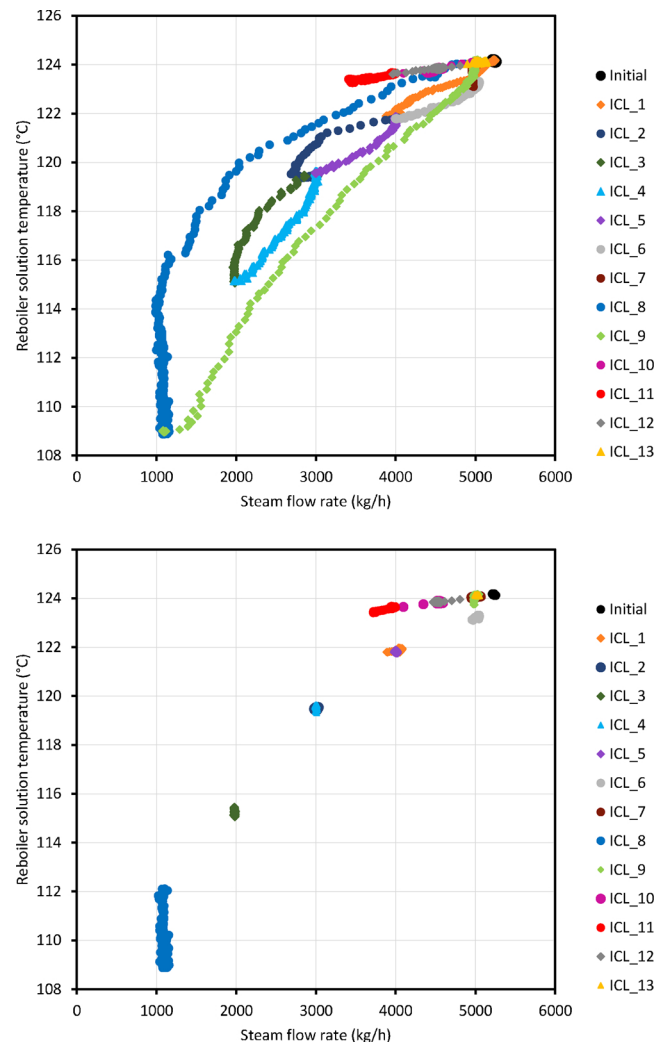


Fig. C.17. The steam pressure valve positioning is adjusted to achieve a certain steam flow rate, which in turn, dictates the reboiler temperature. The effect of changing steam flow rate on the reboiler temperature is shown for (Top) the entire flexible operation test campaign, and (Bottom) only the duration of steady state operation, where the colour of the markers indicate the time period (i.e., from Initial and ICL_1 to ICL_13). The reboiler temperature during steady state operation is constant for almost all of the time periods. However, there is variation in reboiler temperature during the “steady state” period of ICL_8 due to fluctuations occurring at the steam pressure valve. Note: this test campaign used a welded plate thermosiphon heat exchanger (CHP configuration of the TCM plant).

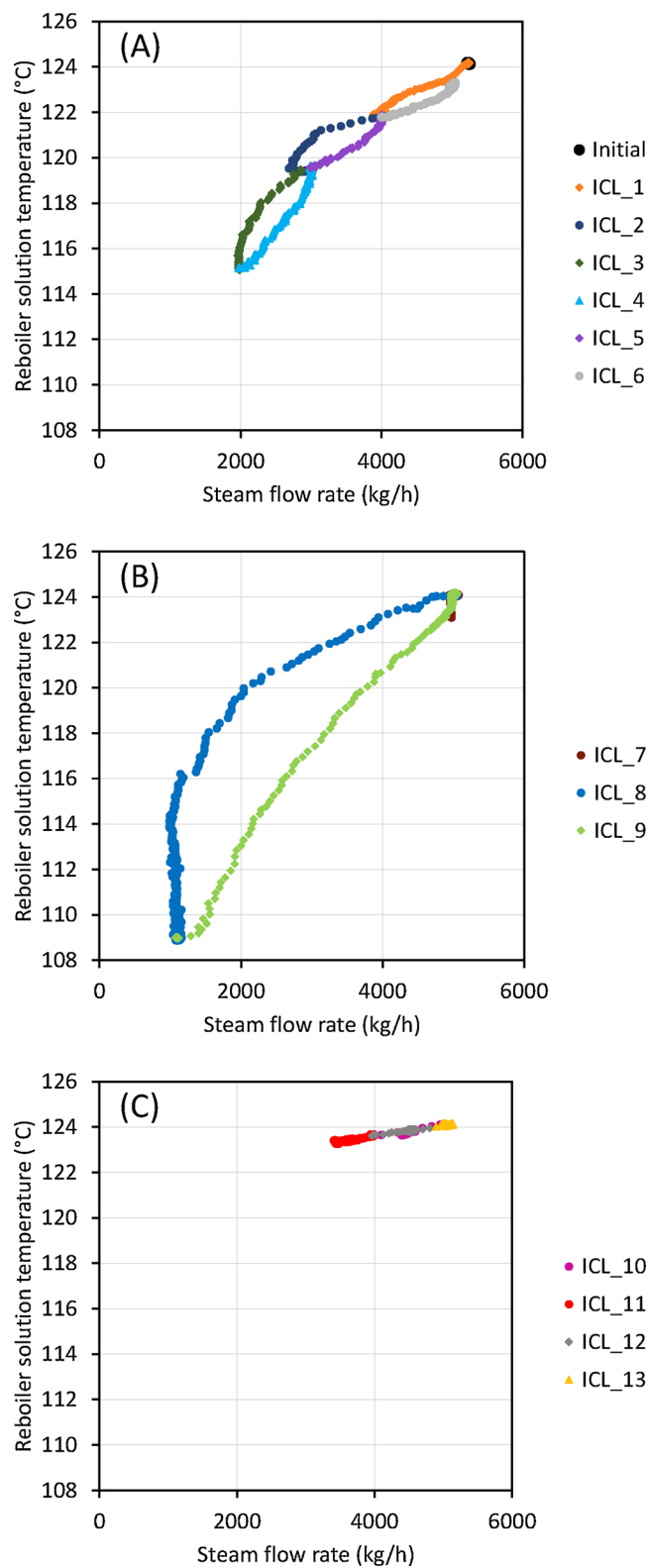


Fig. C.18. The effect of changing steam flow rate on the reboiler temperature during the scenarios: (A) effect of steam flow rate, (B) time-varying solvent regeneration, and (C) variable ramp rate. From observing Fig. 2, it is apparent that most time periods with decreasing steam flow rate have more convex reboiler temperature profiles (ICL_1 to ICL_3, ICL_7). The reboiler temperature profiles for time periods with increasing steam flow rate are less convex (ICL_9) or even concave (ICL_4 to ICL_6). In the variable ramp rate scenario (ICL_10 to ICL_13), the magnitude of change in steam flow rate was not large enough to vary reboiler temperature.

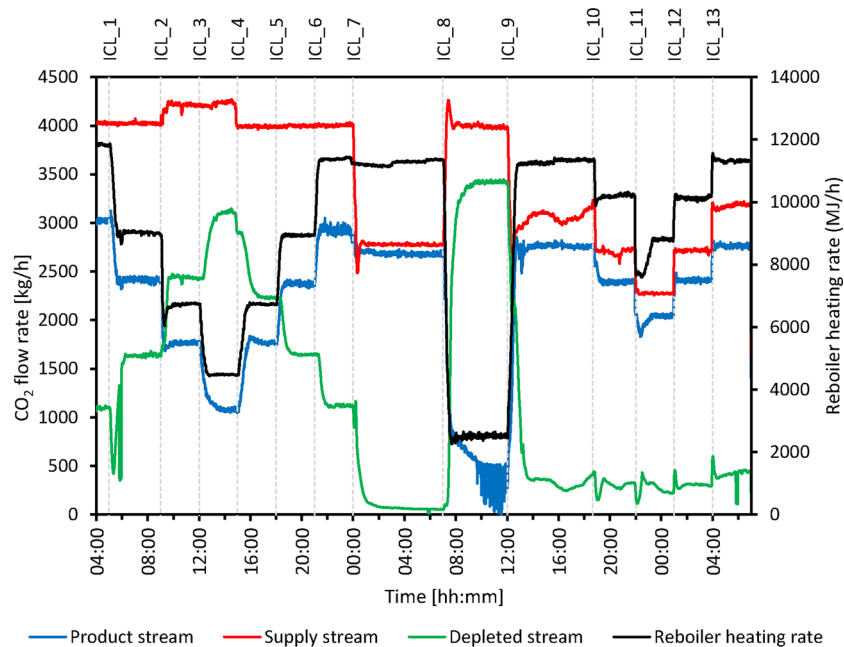
C.5 CO₂ mass flows and cumulative CO₂ capture rate

Fig. C.19. The CO₂ mass flow rate in the supply stream (absorber inlet), depleted flue gas stream (absorber outlet) and the CO₂ product stream (stripper outlet). The black line shows the reboiler heating rate (MJ/h).

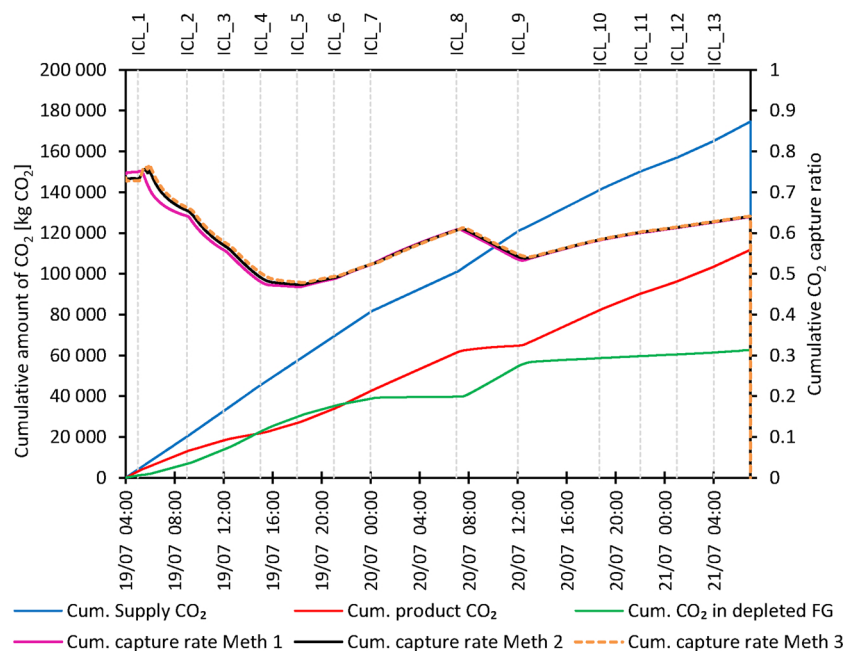


Fig. C.20. Cumulative amount of CO₂ in the gas streams over the course of the TCM test campaign (i.e., supply stream, product stream and depleted flue gas stream). These cumulative values are used to calculate the cumulative CO₂ capture rate in tables C.15 and C.16 (using calculation methods 1–3 in Table B.4).

Table C.15

Cumulative mass of CO₂ of each gas stream and the cumulative capture rate for each time period over the course of the TCM test campaign. These cumulative values are used to calculate the cumulative CO₂ capture rate (calculation methods 1–3 shown in Table B.4). Method 4 CO₂ capture rate is not applicable for cumulative CO₂ calculations.

	Initial	ICL_1	ICL_2	ICL_3	ICL_4	ICL_5	ICL_6	ICL_7	ICL_8	ICL_9	ICL_10	ICL_11	ICL_12	ICL_13
Cumulative supply CO ₂ (kg)	3993.2	16,094.5	12,594.1	12,647.6	11,974.1	11,989.2	12,011.9	19,561.8	19,835.5	20,345.1	9105.3	6835.6	8171.8	9527.2
Cumulative product CO ₂ (kg)	2995.7	9904.6	5365.9	3552.6	5016.6	6953.7	8679.6	18,832.6	3411.3	17,414.8	8070.0	6040.3	7239.7	8289.9
Cumulative CO ₂ in depleted FG (kg)	1086.9	5686.1	6972.4	8789.3	7265.8	5310.9	3642.9	958.8	14,778.6	4196.1	1007.1	803.9	935.5	1230.9
CO ₂ ± by end of time period (kg)	−89.4	503.8	255.9	305.7	−308.3	−275.4	−310.5	−229.6	1645.5	−1265.8	28.1	−8.6	−3.3	6.4
CO ₂ stored inside solvent end of time period (kg)	2080.4	2584.2	2840.1	3145.8	2837.5	2562.1	2251.5	2022.0	3667.5	2401.7	2429.8	2421.2	2417.8	2424.2
<i>Cumulative CO₂ capture rate (%)</i>														
Method 1 (%)	75.02	61.54	42.61	28.09	41.90	58.00	72.26	96.27	17.20	85.60	88.63	88.37	88.59	87.01
Method 2 (%)	73.38	63.53	43.49	28.78	40.84	56.70	70.44	95.16	18.75	80.58	88.90	88.25	88.56	87.07
Method 3 (%)	72.78	64.67	44.64	30.51	39.32	55.70	69.67	95.10	25.49	79.38	88.94	88.24	88.55	87.08
Average cumulative CO ₂ capture rate (%)	73.7	63.2	43.6	29.1	40.7	56.8	70.8	95.5	20.5	81.9	88.8	88.3	88.6	87.1

Table C.16

Cumulative mass of CO₂ based on the gas stream flow rate and the “stored” CO₂ for each test scenario. The cumulative CO₂ values are used to calculate the cumulative CO₂ capture rate (methods 1–3 in Table B.4). Method 4 CO₂ capture rate is not applicable for cumulative CO₂ calculations.

	Effect of steam flow rate ICL_1 to ICL_6	Time-varying solvent regen ICL_7 to ICL_9	Variable ramp rate ICL_10 to ICL_13	Over entire test campaign ICL_1 to ICL_13
Cumulative supply CO ₂ (kg)	77,311.5	59,742.3	33,639.9	174,686.9
Cumulative product CO ₂ (kg)	39,473.0	39,658.7	29,639.9	111,767.3
Cumulative CO ₂ in depleted FG (kg)	37,667.3	19,933.5	3977.4	62,665.1
<i>Cumulative CO₂ capture rate (%)</i>				
Method 1 (%)	51.06	66.38	88.11	63.98
Method 2 (%)	51.17	66.55	88.17	64.07
Method 3 (%)	51.28	66.63	88.18	64.13
Average cumulative CO ₂ capture rate (%)	51.2	66.5	88.2	64.1

Appendix D. Data noise removal using Origin

From a practical operability perspective, noise should not simply be disregarded and the possible cause/source should be considered (e.g., poor positioning of a probe, electrical noise, mechanical vibration, process noise). However, to have useable data for modelling purposes and to calculate performance indicators (e.g., specific reboiler duty, CO₂ capture rate), smoothing noise is necessary. This section describes techniques used to remove noise from data.

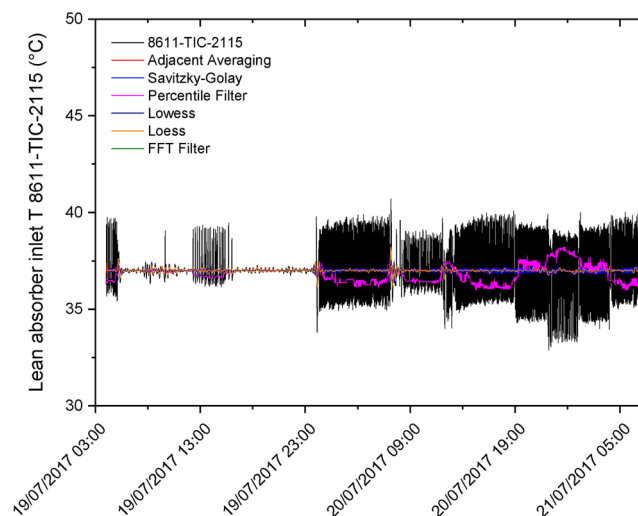


Fig. D.21. Different smoothing methods is applied to the temperature transmitter 8611-TIC-2115 data (black line), which shows significant noise at certain process conditions. The window size for Adjacent Averaging, Savitzky–Golay, Percentile Filter, and FFT Filter is 80 points, whereas 62 points (span 0.01) was used with Lowess and Loess.

The Origin graphing and data analysis tool was used to smooth noisy pilot plant data. Figs D.21 and D.22 demonstrate the effect of different smoothing methods and the effect of “window size” or span (i.e., the proportion of points used to calculate the smoothed value). An overview of the smoothing methods available in Origin is provided below.

The **Savitzky–Golay** (SG) method performs a local polynomial regression around each point, which preserves the shape of the peaks. The SG approach is often called a digital smoothing polynomial filter or a least-squares smoothing filter (MathWorks, 2018). The **Adjacent Averaging** method replaces each point with the average of a user-specified number of points (i.e., window size) around each particular point. It provides wide smoothing and is suitable for smoothing data with wider peaks, however may “wash out” features of the data. Both the Savitzky–Golay and Adjacent Averaging methods are suitable for background noise removal, where dataset contains noise with normal distribution (Origin, 2019).

The **Percentile Filter** method (e.g., 50% percentile filter or median filter) replaces the value at each point with the median value of a group of surrounding points. The Percentile Filter eliminates the noise with abnormal amplitude, however, it should be only used on data with shot noise, i.e., noise appears as localised spikes (Origin, 2019). As the noise in the 8611-TIC-2115 dataset has numerous spikes occurring successively, the Percentile Filter is incompatible with this dataset (Fig. D.21 Fig. D.21). The **FFT filter** is used to remove high-frequency noise, leaving the true signal after application (Origin, 2019).

The **Lowess** and **Loess** methods use locally weighted linear regression, abbreviated from “locally weighted scatterplot smoothing” or “locally

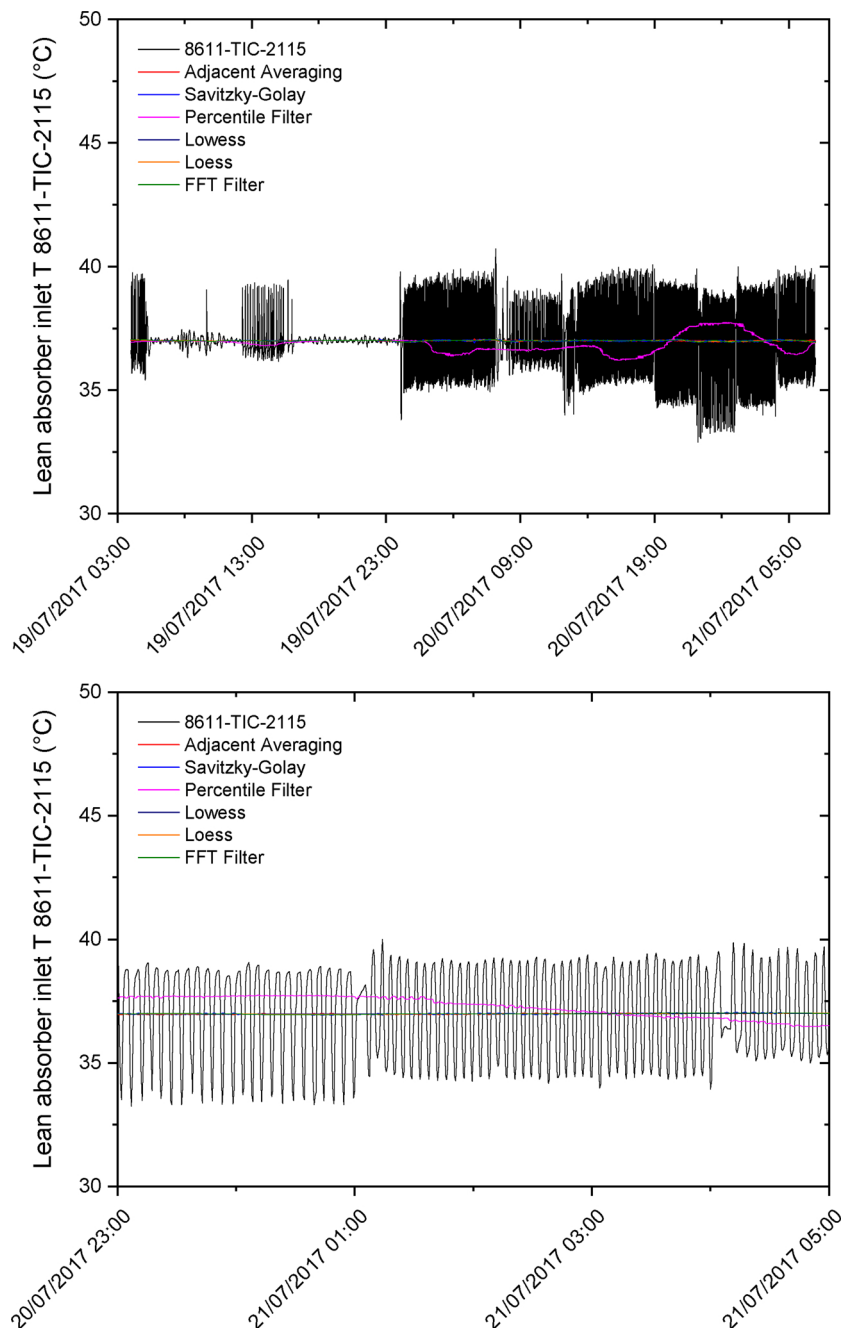


Fig. D.22. Different smoothing methods is applied to the temperature transmitter 8611-TIC-2115 data (black line), which shows significant noise at certain process conditions. The window sizes used to achieve smoothing: 400 points with Adjacent Averaging, Savitzky–Golay; 600 point with Percentile Filter, Lowess and Loess; and 100 points with the FFT Filter. (Top) Smoothing over the full dataset. (Bottom) Zooming in on the data between 20/7/2017 23:00 to 2/7/2017 05:00.

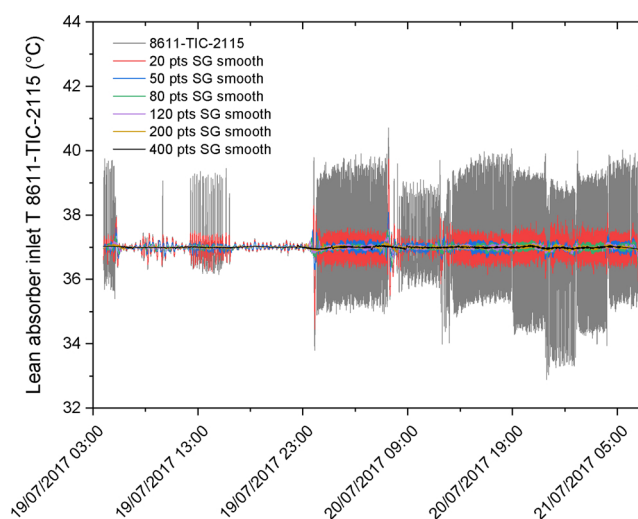


Fig. D.23. The effect of different numbers for window size on data smoothing of the temperature transmitter 8611-TIC-2115 measurement when using the Savitzky–Golay filter. The window size is the number of user-specified points used in each local regression.

weighted least squares”. Each smoothed value is determined using adjacent data points defined within the span. The span is specified as a number between 0 and 1, which corresponds to a proportion of points, e.g., span of 0.1 would use 10% of the data points. The regression weight function is defined using different models in the regression, Lowess uses a linear polynomial, whereas Loess uses a quadratic polynomial (MathWorks, 2018; Origin, 2019). **Binomial filter** is a weighted moving average filters and is considered to be a low-pass filter to remove high frequency noise. For this method, the weight is derived from binomial coefficients. The Binomial filter and the Lowess/Loess smoothing methods can be used to detect trends in noisy data, particularly useful for a large number of data points (Origin, 2019).

The “window size” or “span” is the number/proportion of data points used in each local regression or average calculation. Increasing the “window size” increases the smoothness of the result (Fig. D.23). For all smoothing methods, the effect of window size is illustrated in the comparison between Fig. D.21 and D.22. In general, it is expected that at very large window sizes, the Adjacent Averaging and Percentile Filter methods would significantly deviate from the input signal. As the Savitzky–Golay filter preserves the features of the data (e.g., peak height and width) and overall profile, SG is considered superior compared to the Adjacent Averaging method and Percentile Filter (Origin, 2019).

References

- Abdilahi, A.M., Mustafa, M.W., Abujarad, S.Y., Mustapha, M., 2018. Harnessing flexibility potential of flexible carbon capture power plants for future low carbon power systems: review. *Renew. Sustain. Energy Rev.* 81, 3101–3110.
- Alobaid, F., Mertens, N., Starkloff, R., Lanz, T., Heinze, C., Eppel, B., 2017. Progress in dynamic simulation of thermal power plants. *Prog. Energy Combust. Sci.* 59, 79–162.
- Andersson, V., Wittmeyer, K., Gorset, O., Maree, Y., Sanden, K., 2013. Operational experience and initial results from the first test period at CO₂ Technology Centre Mongstad. *Energy Proc.* 37, 6348–6356.
- Bandyopadhyay, R., Patiño-Echeverri, D., 2016. An alternate wind power integration mechanism: coal plants with flexible amine-based CCS. *Renew. Energy* 85, 704–713.
- Bernhardsen, I.M., Knuutila, H.K., 2017. A review of potential amine solvents for CO₂ absorption process: absorption capacity, cyclic capacity and pKa. *Int. J. Greenhouse Gas Control* 61, 27–48.
- Biliyok, C., Lawal, A., Wang, M., Seibert, F., 2012. Dynamic modelling, validation and analysis of post-combustion chemical absorption CO₂ capture plant. *Int. J. Greenhouse Gas Control* 9, 428–445.
- Billet, R., Schultes, M., 1993. Predicting mass transfer in packed columns. *Chem. Eng. Technol.* 16 (1), 1–9.
- Boston, A., Thomas, H.K., 2015. Managing Flexibility Whilst Decarbonising the GB Electricity System. Tech. Rep. <http://eruk.org/project/managing-flexibility-of-the-electricity-system/>.
- Brand, C.V., Rodríguez, J., Galindo, A., Jackson, G., Adjiman, C.S., 2012. Validation of an absorber model of carbon dioxide capture in an aqueous amine solvent developed based on the SAFT-VR framework. *Comput. Aided Chem. Eng.* 31, 930–934.
- Brand, C.V., 2013. CO₂ capture using monoethanolamine solutions: Development and validation of a process model based on the SAFT-VR equation of state, PhD thesis. Department of Chemical Engineering, Imperial College London, UK. <https://core.ac.uk/download/pdf/76988588.pdf>.
- Brigman, N., Shah, M.I., Falk-Pedersen, O., Cents, T., Smith, V., de Cazenove, T., Morken, A.K., Hvidsten, O.A., Chhaganlal, M., Feste, J.K., Lombardo, G., Bade, O.M., Knudsen, J., Subramoney, S.C., Fostås, B.F., Koeijer, G.d., Hamborg, E.S., 2014. Results of amine plant operations from 30 wt% and 40 wt% aqueous MEA testing at the CO₂ Technology Centre Mongstad. *Energy Proc.* 63, 6012–6022.
- Bui, M., Gunawan, I., Verheyen, V., Feron, P., Meuleman, E., Adeloju, S., 2014a. Dynamic modelling and optimisation of flexible operation in post-combustion CO₂ capture plants – a review. *Comput. Chem. Eng.* 61, 245–265.
- Bui, M., Gunawan, I., Verheyen, T.V., Meuleman, E., Feron, P., 2014b. Dynamic operation of post-combustion CO₂ capture in Australian coal-fired power plants. *Energy Proc.* 63, 1368–1375.
- Bui, M., Gunawan, I., Verheyen, V., Feron, P., Meuleman, E., 2016a. Flexible operation of CSIRO’s post-combustion CO₂ capture pilot plant at the AGL Loy Yang power station. *Int. J. Greenhouse Gas Control* 48 (Part 2), 188–203 (Flexible operation of carbon capture plants).
- Bui, M., Gunawan, I., Verheyen, V., Meuleman, E., 2016b. Dynamic operation of liquid absorbent-based postcombustion CO₂ capture plants. *Absorption-Based Post-combustion Capture of Carbon Dioxide*. Woodhead Publishing, Cambridge.
- Bui, M., Adjiman, C.S., Bardow, A., Anthony, E.J., Boston, A., Brown, S., Fennell, P., Fuss, S., Galindo, A., Hackett, L.A., Hallett, J.P., Herzog, H.J., Jackson, G., Kemper, J., Krevor, S., Maitland, G.C., Matuszewski, M., Metcalfe, I.S., Petit, C., Puxty, G., Reimer, J., Reiner, D.M., Rubin, E.S., Scott, S.A., Shah, N., Smit, B., Trusler, J.P.M., Webley, P., Wilcox, J., Mac Dowell, N., 2018a. Carbon capture and storage (CCS): the way forward. *Energy Environ. Sci.* 11 (5), 1062–1176.
- Bui, M., Tait, P., Lucquiaud, M., Mac Dowell, N., 2018b. Dynamic operation and modelling of amine-based CO₂ capture at pilot scale. *Int. J. Greenhouse Gas Control* 79, 134–153.
- Chalmers, H., Gibbins, J., 2007. Initial evaluation of the impact of post-combustion capture of carbon dioxide on supercritical pulverised coal power plant part load performance. *Fuel* 86 (14), 2109–2123.
- Chapman, W.G., Gubbins, K.E., Jackson, G., Radosz, M., 1989. SAFT: equation-of-state solution model for associating fluids. *Fluid Phase Equilib.* 52, 31–38.
- Chapman, W.G., Gubbins, K.E., Jackson, G., Radosz, M., 1990. New reference equation of state for associating liquids. *Ind. Eng. Chem. Res.* 29 (8), 1709–1721.
- Cohen, S.M., Rochelle, G.T., Webber, M.E., 2012. Optimizing post-combustion CO₂ capture in response to volatile electricity prices. *Int. J. Greenhouse Gas Control* 8, 180–195.
- de Koeijer, G.M., Aasen, K.I., Hamborg, E.S., 2014. Scale-up and transient operation of CO₂ capture plants at CO₂ Technology Centre Mongstad. Abu Dhabi International Petroleum Exhibition and Conference, Society of Petroleum Engineers, Paper SPE-171873.
- Enaasen, N., Zangrilli, L., Mangiaracina, A., Mejdell, T., Kvamsdal, H.M., Hillestad, M., 2014. Validation of a dynamic model of the Brindisi pilot plant. *Energy Proc.* 63, 1040–1054.
- Flø, N.E., Knuutila, H., Kvamsdal, H.M., Hillestad, M., 2015. Dynamic model validation of the post-combustion CO₂ absorption process. *Int. J. Greenhouse Gas Control* 41, 127–141.
- Faramarzi, L., Thimsen, D., Hume, S., Maxon, A., Watson, G., Pedersen, S., Gjernes, E., Fostås, B.F., Lombardo, G., Cents, T., Morken, A.K., Shah, M.I., de Cazenove, T.,

- Hamborg, E.S., 2017. Results from MEA testing at the CO₂ Technology Centre Mongstad: verification of baseline results in 2015. *Energy Proc.* 114, 1128–1145.
- Flø, N.E., Kvamsdal, H.M., Hillestad, M., 2016. Dynamic simulation of post-combustion CO₂ capture for flexible operation of the Brindisi pilot plant. *Int. J. Greenhouse Gas Control* 48 (Part 2), 204–215.
- Flø, N.E., Faramarzi, L., de Cazenove, T., Hvidsten, O.A., Morken, A.K., Hamborg, E.S., Vernstad, K., Watson, G., Pedersen, S., Cents, T., Fostås, B.F., Shah, M.I., Lombardo, G., Gjernes, E., 2017. Results from MEA degradation and reclaiming processes at the CO₂ technology centre Mongstad. *Energy Proc.* 114, 1307–1324.
- Flø, N.E., Faramarzi, L., Iversen, F., Kleppe, E.R., Graver, B., Bryntesen, H.N., Johnsen, K., 2019. Assessment of material selection for the CO₂ absorption process with aqueous MEA solution based on results from corrosion monitoring at Technology Centre Mongstad. *Int. J. Greenhouse Gas Control* 84, 91–110.
- Galindo, A., Davies, L.A., Gil-Villegas, A., Jackson, G., 1998. The thermodynamics of mixtures and the corresponding mixing rules in the SAFT-VR approach for potentials of variable range. *Mol. Phys.* 93 (2), 241–252.
- Garðarsdóttir, S.O., Normann, F., Andersson, K., Prölß, K., Emilsdóttir, S., Johnsson, F., 2015. Post-combustion CO₂ capture applied to a state-of-the-art coal-fired power plant – the influence of dynamic process conditions. *Int. J. Greenhouse Gas Control* 33, 51–62.
- Gil-Villegas, A., Galindo, A., Whitehead, P.J., Mills, S.J., Jackson, G., Burgess, A.N., 1997. Statistical associating fluid theory for chain molecules with attractive potentials of variable range. *J. Chem. Phys.* 106 (10), 4168–4186.
- Hamborg, E.S., Smith, V., Cents, T., Brigman, N., Pedersen, O.F., de Cazenove, T., Chhaganlal, M., Feste, J.K., Ullestad, O., Ulvatn, H., Gorset, O., Askestad, I., Gram, L.K., Fostås, B.F., Shah, M.I., Maxson, A., Thimsen, D., 2014. Results from MEA testing at the CO₂ Technology Centre Mongstad. Part II. Verification of baseline results. *Energy Proc.* 63, 5994–6011.
- Hentschel, J., Babić, U., Spliethoff, H., 2016. A parametric approach for the valuation of power plant flexibility options. *Energy Rep.* 2, 40–47.
- Heuberger, C.F., Mac Dowell, N., 2018. Real-world challenges with a rapid transition to 100% renewable power systems. *Joule* 2 (3), 367–370.
- Heuberger, C.F., Staffell, I., Shah, N., Mac Dowell, N., 2016. Quantifying the value of CCS for the future electricity system. *Energy Environ. Sci.* 9 (8), 2497–2510.
- Heuberger, C.F., Mac Dowell, N., Staffell, I., Shah, N., 2017a. IEAGHG Technical Report 2017-09: Valuing Flexibility in CCS Power Plants, Report. International Energy Agency Greenhouse Gas R&D Programme (IEAGHG). http://www.ieaghg.org/exco_docs/2017-09.pdf.
- Heuberger, C.F., Rubin, E.S., Staffell, I., Shah, N., Mac Dowell, N., 2017b. Power capacity expansion planning considering endogenous technology cost learning. *Appl. Energy* 204 (Suppl. C), 831–845.
- Heuberger, C.F., Staffell, I., Shah, N., Mac Dowell, N., 2017c. A systems approach to quantifying the value of power generation and energy storage technologies in future electricity networks. *Comput. Chem. Eng.* 107 (Suppl. C), 247–256.
- Husebye, J., Anantharaman, R., Fleten, S.-E., 2011. Techno-economic assessment of flexible solvent regeneration & storage for base load coal-fired power generation with post combustion CO₂ capture. *Energy Proc.* 4, 2612–2619.
- IPCC, 2018. Global Warming of 1.5 °C, an IPCC Special Report on the Impacts of Global Warming of 1.5 °C. Intergovernmental Panel on Climate Change. <http://www.ipcc.ch/report/sr15/>.
- Knudsen, J.N., Jensen, J.N., Vilhelmsen, P.-J., Biede, O., 2009. Experience with CO₂ capture from coal flue gas in pilot-scale: testing of different amine solvents. *Energy Proc.* 1 (1), 783–790.
- Koch-Glitsch, 2010. Intalox Packed Tower Systems – Structured Packing. USA. <http://www.koch-glitsch.com/masstransfer/pages/INTALOX-PACKED-TOWER-SYSTEMS.aspx>.
- Kvamsdal, H.M., Rochelle, G.T., 2008. Effects of the temperature bulge in CO₂ absorption from flue gas by aqueous monoethanolamine. *Ind. Eng. Chem. Res.* 47 (3), 867–875.
- Lafitte, T., Apostolou, A., Avendaño, C., Galindo, A., Adjiman, C.S., Müller, E.A., Jackson, G., 2013. Accurate statistical associating fluid theory for chain molecules formed from Mie segments. *J. Chem. Phys.* 139 (15), 154504.
- Ludig, S., Haller, M., Bauer, N., 2010. Tackling long-term climate change together: the case of flexible CCS and fluctuating renewable energy. *Energy Proc.* 4, 2580–2587.
- Mac Dowell, N., Shah, N., 2015. The multi-period optimisation of an amine-based CO₂ capture process integrated with a super-critical coal-fired power station for flexible operation. *Comput. Chem. Eng.* 74, 169–183.
- Mac Dowell, N., Staffell, I., 2016. The role of flexible CCS in the UK's future energy system. *Int. J. Greenhouse Gas Control* 48 (Part 2), 327–344 (Flexible operation of carbon capture plants).
- Mac Dowell, N., Llovel, F., Adjiman, C.S., Jackson, G., Galindo, A., 2010. Modeling the fluid phase behavior of carbon dioxide in aqueous solutions of monoethanolamine using transferable parameters with the SAFT-VR approach. *Ind. Eng. Chem. Res.* 49 (4), 1883–1899.
- Mac Dowell, N., Pereira, F.E., Llovel, F., Blas, F.J., Adjiman, C.S., Jackson, G., Galindo, A., 2011. Transferable SAFT-VR models for the calculation of the fluid phase equilibria in reactive mixtures of carbon dioxide, water, and n-alkylamines in the context of carbon capture. *J. Phys. Chem. B* 115 (25), 8155–8168.
- Mangiaracina, A., Zangrilli, L., Robinson, L., Kvamsdal, H.M., Van Os, P., 2014. OCTAVIUS: evaluation of flexibility and operability of amine based post combustion CO₂ capture at the Brindisi pilot plant. *Energy Proc.* 63, 1617–1636.
- MathWorks, 2018. Curve Fitting Toolbox™ User's Guide: Chapter 6 Interpolation and Smoothing – Filtering and Smoothing Data. MathWorks Inc, US (Accessed 14 March 2019). https://uk.mathworks.com/help/curvefit/smoothing-data.html#bq_6zbc.
- Mechleri, E., Fennell, P.S., Mac Dowell, N., 2017. Optimisation and evaluation of flexible operation strategies for coal- and gas-CCS power stations with a multi-period design approach. *Int. J. Greenhouse Gas Control* 59, 24–39.
- Miller, B.G., 2017. Part 2: Coal Utilization Technologies, Clean Coal Engineering Technology, 2nd ed. Butterworth-Heinemann, Elsevier.
- Montañés, R., Flø, N.E., Nord, L., 2017. Dynamic process model validation and control of the amine plant at CO₂ Technology Centre Mongstad. *Energies* 10 (10), 1527.
- Montañés, R.M., Flø, N.E., Nord, L.O., 2018. Experimental results of transient testing at the amine plant at Technology Centre Mongstad: open-loop responses and performance of decentralized control structures for load changes. *Int. J. Greenhouse Gas Control* 73, 42–59.
- Morken, A.K., Pedersen, S., Nesse, S.O., Flø, N.E., Johnsen, K., Feste, J.K., de Cazenove, T., Faramarzi, L., Vernstad, K., 2019. CO₂ capture with monoethanolamine: solvent management and environmental impacts during long term operation at the Technology Centre Mongstad (TCM). *Int. J. Greenhouse Gas Control* 82, 175–183.
- Oates, D.L., Versteeg, P., Hittinger, E., Jaramillo, P., 2014. Profitability of CCS with flue gas bypass and solvent storage. *Int. J. Greenhouse Gas Control* 27, 279–288.
- Origin, 2019. Signal Processing: Smoothing. OriginLab (Accessed 14 March 2019). <https://www.originlab.com/doc/Origin-Help/Smoothing>.
- Papaoannou, V., Lafitte, T., Avendaño, C., Adjiman, C.S., Jackson, G., Müller, E.A., Galindo, A., 2014. Group contribution methodology based on the statistical associating fluid theory for heteronuclear molecules formed from Mie segments. *J. Chem. Phys.* 140 (5), 054107.
- PSE, 2016. gCCS Model Documentation. Process Systems Enterprise Ltd, London, UK.
- PSE, 2017. gCCS – Overview. Process Systems Enterprise (Accessed 10 January 2018). <https://www.psentrprise.com/products/gccs>.
- Raksajati, A., Ho, M.T., Wiley, D.E., 2013. Reducing the cost of CO₂ capture from flue gases using aqueous chemical absorption. *Ind. Eng. Chem. Res.* 52 (47), 16887–16901.
- Rodríguez, J., Mac Dowell, N., Llovel, F., Adjiman, C.S., Jackson, G., Galindo, A., 2012. Modelling the fluid phase behaviour of aqueous mixtures of multifunctional alkanolamines and carbon dioxide using transferable parameters with the SAFT-VR approach. *Mol. Phys.* 110 (11–12), 1325–1348.
- Rodríguez, J., Andrade, A., Lawal, A., Samsati, N., Calado, M., Ramos, A., Lafitte, T., Fuentes, J., Pantelides, C.C., 2014. An integrated framework for the dynamic modelling of solvent-based CO₂ capture processes. *Energy Proc.* 63, 1206–1217.
- Seebregts, A.J., 2010 April. Gas-Fired Power, Energy Technology Systems Analysis Programme – Technology Brief E02. IEA Energy Technology Network. <https://iea-etsap.org/E-TechDS/PDF/E02-gas-fired-power-GS-AD-gct.pdf>.
- Tait, P., Buschle, B., Ausner, I., Valluri, P., Wehrli, M., Lucquiaud, M., 2016. A pilot-scale study of dynamic response scenarios for the flexible operation of post-combustion CO₂ capture. *Int. J. Greenhouse Gas Control* 48 (2), 216–233.
- Tait, P., Buschle, B., Milkowski, K., Akram, M., Pourkashanian, M., Lucquiaud, M., 2017. Demonstration of CO₂ capture rate control at pilot scale using continuous online solvent measurements. In: 9th Trondheim Conference on CO₂ Capture, Transport and Storage. 12–14 June 2017, Trondheim, Norway.
- Tait, P., Buschle, B., Milkowski, K., Akram, M., Pourkashanian, M., Lucquiaud, M., 2018. Flexible operation of post-combustion CO₂ capture at pilot scale with demonstration of capture-efficiency control using online solvent measurements. *Int. J. Greenhouse Gas Control* 71, 253–277.
- Thimsen, D., Maxson, A., Smith, V., Cents, T., Falk-Pedersen, O., Gorset, O., Hamborg, E.S., 2014. Results from MEA testing at the CO₂ Technology Centre Mongstad. Part I. Post-Combustion CO₂ capture testing methodology. *Energy Proc.* 63, 5938–5958.
- Tontiwachwuthikul, P., Meisen, A., Lim, C.J., 1992. CO₂ absorption by NaOH, monoethanolamine and 2-amino-2-methyl-1-propanol solutions in a packed column. *Chem. Eng. Sci.* 47 (2), 381–390.
- van de Haar, A.M., Trapp, C., Wellner, K., de Kler, R., Schmitz, G., Colonna, P., 2017. Dynamics of post-combustion CO₂ capture plants: modelling, validation and case study. *Ind. Eng. Chem. Res.* 56 (7), 1810–1822.
- van der Wijk, P.C., Brouwer, A.S., van den Broek, M., Slot, T., Stienstra, G., van der Veen, W., Faaij, A.P.C., 2014. Benefits of coal-fired power generation with flexible CCS in a future northwest European power system with large scale wind power. *Int. J. Greenhouse Gas Control* 28, 216–233.
- Van Peteghem, T., Delarue, E., 2014. Opportunities for applying solvent storage to power plants with post-combustion carbon capture. *Int. J. Greenhouse Gas Control* 21, 203–213.
- Zaman, M., Lee, J.H., 2015. Optimization of the various modes of flexible operation for post-combustion CO₂ capture plant. *Comput. Chem. Eng.* 75, 14–27.
- Zaman, M., Jang, H., Rizwan, M., Lee, J.H., 2016. Optimal design for flexible operation of the post-combustion CO₂ capture plant with uncertain economic factors. *Comput. Chem. Eng.* 84, 199–207.
- Zhang, W., Liu, H., Sun, Y., Cakstins, J., Sun, C., Snape, C.E., 2016. Parametric study on the regeneration heat requirement of an amine-based solid adsorbent process for post-combustion carbon capture. *Appl. Energy* 168, 394–405.